Dipyridophenazine Complexes of Os(II) as Red-Emitting DNA Probes: Synthesis, Characterization, and Photophysical Properties

R. Erik Holmlin, Johanna A. Yao, and Jacqueline K. Barton*

Division of Chemistry and Chemical Engineering, California Institute of Technology, Pasadena, California 91125

Received July 28, 1998

Polypyridyl complexes of Os(II) bearing one dipyridophenazine (dppz) derivative and two ancillary ligands derived from bipyridine (bpy) or phenanthroline (phen) exhibit emission maxima at ∼740 nm and average excited-state lifetimes in the 10 ns range upon binding to DNA by preferential intercalation of the dppz ligand. A family of $[Os(L^1)(L^2)(L^3)]^{2+}$ and $[Os(L^1)_2(L^2)]^{2+}$ complexes with simple modifications in the ancillary phen or bpy ligands (L^1 and L^3) as well as the intercalating dppz ligand (L^2) was prepared. By cyclic voltammetry, electron-donating substituents on the ancillary ligands lowered the Os(3+/2+) reduction potential but did not affect the reduction potential of the dppz ligand. A methyl substituent at the 7-, 8-, or 6-position of the dppz ligand shifted the phenazine reduction toward the negative but did not affect the Os(3+/2+) potential. Absorption titrations indicated intercalative binding to DNA with high affinity (K_B ∼10^6 M^{-1}) for the family of complexes, although at high ratios (50:1) of base pairs to metal, complexes with ancillary 4,7-dimethylphenanthroline or 4,4′-dimethylbipyridine ligands exhibit less hypochromism (26−27%) in the $\pi-\pi^*$ transition on the dppz ligand compared to complexes with 5,6-dimethylphenanthroline (30−37%) or the parent phen (31−35%). By steady-state and time-resolved emission spectroscopy, complexes bound to DNA by intercalation with substituents on the 4,7- or 4,4′-positions of the ancillary phen or bpy displayed lower quantum yields for emission (Φ_{em}) compared to complexes with the parent phen, while complexes with methyl substituents on the dppz ligand had the greatest Φ_{em}. Studies with poly d(AT), poly d(GC), and mixed-sequence DNA revealed that the emission yields are also sequence-dependent. Comparative luminescence studies in CH_2Cl_2 demonstrated that these effects arise from a combination of (i) the inherent sensitivity of the excited state to ligand structure and (ii) perturbations in DNA binding geometry introduced by substituents on the ancillary and intercalating ligands. Our results clarify the relationships between ligand architecture and emission yield and lifetime in the presence and absence of DNA and illustrate the utility of dppz complexes of Os(II) as luminescent probes for DNA.

Introduction

Transition metal complexes that bind to DNA and RNA by intercalation, metallointercalators, represent an important class of molecular probes. Metallointercalators based on ruthenium(II) and rhodium(III) have been useful in studies of nucleic acid structure and function.[1,2] As part of an ongoing effort to develop new and effective diagnostics for nucleic acids in solution, we carried out an investigation of dipyridophenazine complexes of osmium(II) as a new class of red-emitting DNA probes.

Dipyridophenazine complexes of Os(II),[3,4] Ru(II),[5,6] and Re(I)[7,8] provide sensitive luminescent probes for double-helical DNA in solution. Despite readily detectable luminescence in organic solvents, emission from photoexcited $[M(L)_2(dppz)]^{2+}$ (M = Os, Ru; L = bpy, phen; dppz = dipyrido[3,2-*a*:2′,3′-*c*]-phenazine) is quenched in aqueous solution by the interaction of protons of the solvent with the phenazine nitrogens of the dppz ligand.[9] For the Re(I)[7,8] complex, intersystem crossing (ISC) to a $\pi-\pi^*$ transition on the dppz ligand deactivates the emission. Upon binding to DNA by preferential intercalation of the dppz ligand between adjacent DNA base pairs, these processes are inhibited, and the complexes emit. The emission profile of these dppz complexes is sensitive to solvent accessibility, which makes them excellent molecular probes. In fact, dppz complexes of ruthenium have been used to probe hydrophobic matrices in aqueous solution other than DNA such as Nafion[10] films and SDS micelles.[11]

A limited number of detailed investigations have been directed at elucidating the mechanism that accounts for the quenching of photoexcited dppz complexes of Ru(II) by water.[12,13] Turro et al. examined quenching by proton donors

* To whom correspondence should be addressed.

(1) Johann, T. W.; Barton, J. K. *Philos. Trans. R. Soc. London A.* **1996**, *354*, 299−324.
(2) (a) Murphy, C. J.; Barton, J. K. *Methods Enzymol.* **1993**, *226*, 576−594. (b) Chow, C.; Barton, J. K. *Methods Enzymol.* **1992**, *212*, 219−242.
(3) Holmlin, R. E.; Barton, J. K. *Inorg. Chem.* **1995**, *34*, 7−8.
(4) Holmlin, R. E.; Stemp, E. D. A.; Barton, J. K. *J. Am. Chem. Soc.* **1996**, *118*, 5236−5244.
(5) Friedman, A. E.; Chambron, J.-C.; Sauvage, J.-P.; Turro, N. J.; Barton, J. K. *J. Am. Chem. Soc.* **1990**, *112*, 4960−4962.
(6) Jenkins, Y.; Friedman, A. E.; Turro, N. J.; Barton, J. K. *Biochemistry* **1992**, 10809−10816.
(7) Stoeffler, H. D.; Thornton, N. B.; Temkin, S. L.; Schanze, K. S. *J. Am. Chem. Soc.* **1995**, *117*, 7119−7128.
(8) Yam, V. W.-W.; Lo, K. K.-W.; Cheung, K.-K.; Kong, R. Y.-C. *J. Chem. Soc., Chem. Commun.* **1995**, 1191−1193.
(9) Amouyal, E.; Homsi, A.; Chambron, J.-C.; Sauvage, J.-P. *J. Chem. Soc., Dalton Trans.* **1990**, 1841−1845.
(10) Sabatani, E.; Nikol, H. D.; Gray, H. B.; Anson, F. C. *J. Am. Chem. Soc.* **1996**, *118*, 1158−1163.
(11) Chambron, J.-C.; Sauvage, J.-P. *Chem. Phys. Lett.* **1991**, *182*, 603−607.
(12) Turro, C.; Bossmann, S. H.; Jenkins, Y.; Barton, J. K.; Turro, N. J. *J. Am. Chem. Soc.* **1995**, *117*, 9026−9032.

10.1021/ic9808955 CCC: $18.00
Published on Web 12/18/1998

in nonaqueous solution and concluded that a discrete proton transfer to the phenazine nitrogen from a sacrificial donor was responsible for deactivating the emission. Olson et al. described the first observation of steady-state emission from *$[Ru(phen)_2(dppz)]^{2+}$ in water. In their analysis, they concluded that the quenching was the result of intramolecular charge transfer (IMCT) involving the dppz ligand. This IMCT is facilitated by hydrogen bonding to the phenazine nitrogens. In each study, it is clear that interactions between the phenazine nitrogens and protons from the solvent lead to charge transfer onto the dppz ligand and quenching of the emission from the lumiphore.

The luminescence signature of $[Ru(phen)_2(dppz)]^{2+}$ is sensitive to DNA sequence and conformation.[6,17−19] On the basis of comparative luminescence studies of Δ-$[Ru(phen)_2(dppz)]^{2+}$ bound to poly d(AT), poly d(GC), and calf thymus (CT) DNA, we found that this complex binds preferentially to AT sites.[18] Because the complex binds primarily to AT sites, the emission profile of $[Ru(phen)_2(dppz)]^{2+}$ bound to T4 DNA,[19] which is glucosylated in the major groove at GC sites, is not changed relative to native CT at low ratios of metal to DNA. Moreover, groove binding agents that occupy the major groove of DNA displace $[Ru(phen)_2(dppz)]^{2+}$ from the helix, while agents in the minor groove do not induce displacement.

Structural studies of Δ-$[Ru(phen)_2(dppz)]^{2+}$ bound to DNA by ^{1}H NMR indicate that intercalation is from the major groove of DNA, with a family of intercalation geometries.[14,15] This distribution of orientations of the dppz ligand bound to DNA results in differential exposure of the phenazine nitrogens to solvent and accounts for the biexponential decay in emission observed for the racemic complex and the pure enantiomers.[14,15] Hartshorn and Barton found that modifications in the structure of the intercalating ligand caused changes in the emission bound to DNA, which also reflected differences in the orientation of the intercalated complex.[16] Nevertheless, a systematic investigation of the effect of structural changes in the ancillary phen or bpy ligands on the luminescence profiles of dppz complexes bound to DNA has yet to be reported.

$[Os(phen)_2(dppz)]^{2+}$ exhibits identical DNA binding properties but significantly different photophysical and electrochemical properties compared to $[Ru(phen)_2(dppz)]^{2+}$.[3,4] Like the ruthenium complex, $[Os(phen)_2(dppz)]^{2+}$ is also a "molecular light switch" for DNA (Figure 1), and emits in aqueous solution only when the phenazine nitrogens of the dppz ligand are protected, as in intercalation. For the osmium complex, the emission is at long wavelengths ($\lambda_{max} \sim 740$ nm) and the excited-state lifetimes are on the order of 10 ns in the presence of DNA. The Os(III) oxidation state is stabilized by ∼500 mV relative to Ru(III) in related complexes, and because of the large ligand field splitting for the third row transition element, the Os(II) complexes are photochemically much more stable than their ruthenium counterparts.

The low-energy emission of the osmium complexes makes them attractive for applications in biosensing, owing to the large difference in the energy of luminescence from the probe and that of any endogenous fluorescence from the biological matrix. Therefore, DNA binding agents based on the osmium center constitute a unique class of red-emitting DNA probes.

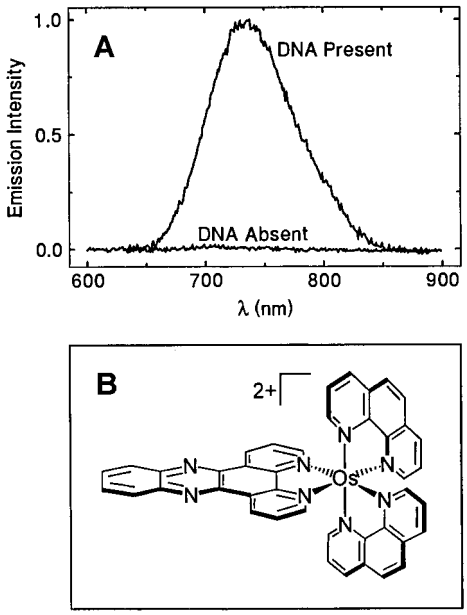

Figure 1. (A) Steady-state emission spectrum of *rac*-$[Os(phen)_2(dppz)]^{2+}$ in the presence and absence of DNA. (B) Schematic illustration of Δ-$[Os(phen)_2(dppz)]^{2+}$. The Δ isomer is shown to illustrate the chirality of the octahedral complex. Conditions: 50 μM Os, 1 mM CT DNA, 5 mM Tris, 50 mM NaCl, pH 8.5.

Here we describe the synthesis and photophysical properties of a family of dppz complexes of Os(II) (Figure 2). We incorporated simple modifications in the ligand architecture of the DNA binding agents and used absorption and emission spectroscopy to determine the relationship between the structure of the ligands that comprise a complex and its emission profile in the presence and absence of DNA. This study provides the first comprehensive characterization of the photophysical and DNA binding properties of dppz complexes of Os(II).

Experimental Section

Materials. Nucleic acid polymers (sonicated, phenol-extracted CT DNA, poly d(AT), and poly d(GC)) were purchased from Pharmacia as lyophilized cakes, dissolved, and exchanged into standard buffer (5 mM Tris, 50 mM NaCl, pH 8.5) by ultrafiltration (Amicon). Phen, 5,6-dmp, 4,7-dmp, and potassium bis-tartratodiantimonate were purchased from Aldrich, $K_2[OsCl_6]$ and $(NH_4)_2[OsCl_6]$ were purchased from Johnson Mathey, and all were used as received. 4-Methyl-4′-butyric acid-2,2′-bipyridyl, 4,4′-dimethoxy-2,2′-bypyridyl, 4,4′-diamino-2,2′-bypyridyl, 1,10-phenanthroline-5,6-dione, and dppz were prepared as described previously.[20,21] $[Os(phen)_2(dppz)](PF_6)_2$ and $[Os(L)_2Cl_2]$ (L = phen, 4,7-dmp, 5,6-dmp, dmob) complexes were also synthesized by established methods.[3,4,22] $[Os(phen)Cl_4]$ was prepared by solid-phase pyrolysis according to the method of Kober et al.[22] Solvents for synthesis were obtained from Aldrich. Solvents for electrochemistry and emission spectroscopy were from Fluka (over molecular sieves). Distilled and deionized water (Millipore: 18 MΩ) was used for all experiments in aqueous solution. Abbreviations used for ligands are as follows: Me_2-dppz = 7,8-dimethyldipyridophenazine; Me-dppz = 6-methyldipyridophenazine; dmob = 4,4′-dimethoxy-2,2′-bipyridyl; 4,7-

(13) Olson, E. J. C.; Hu, D.; Hormann, A.; Jonkman, A. M.; Arkin, M. R.; Stemp, E. D. A.; Barton, J. K.; Barbara, P. F. *J. Am. Chem. Soc.* **1997**, *119*, 11458−11467.
(14) Dupureur, C. M.; Barton, J. K. *J. Am. Chem. Soc.* **1994**, *116*, 10286−10287.
(15) Dupureur, C. M.; Barton, J. K. *Inorg. Chem.* **1997**, *36*, 33−43.
(16) Hartshorn, R. M.; Barton, J. K. *J. Am. Chem. Soc.* **1992**, *114*, 5919−5925.
(17) Friedman, A. E.; Kumar, C. V.; Turro, N. J.; Barton, J. K. *Nucleic Acids Res.* **1991**, *19*, 2595−2602.
(18) Holmlin, R. E.; Stemp, E. D. A.; Barton, J. K. *Inorg. Chem.* **1998**, *37*, 29−34.
(19) Tuite, E.; Lincoln, P.; Nordén, B. *J. Am. Chem. Soc.* **1997**, *119*, 239−240.
(20) Dellaciana, L.; Hamachi, I.; Meyer, T. J. *J. Org. Chem.* **1989**, *54*, 1731−1735.
(21) Dickeson, J. E.; Summers, L. A. *Aust. J. Chem.* **1970**, *23*, 1023−1027.
(22) Kober, E. M.; Caspar, J. V.; Sullivan, B. P.; Meyer, T. J. *Inorg. Chem.* **1988**, *27*, 4587−4598.

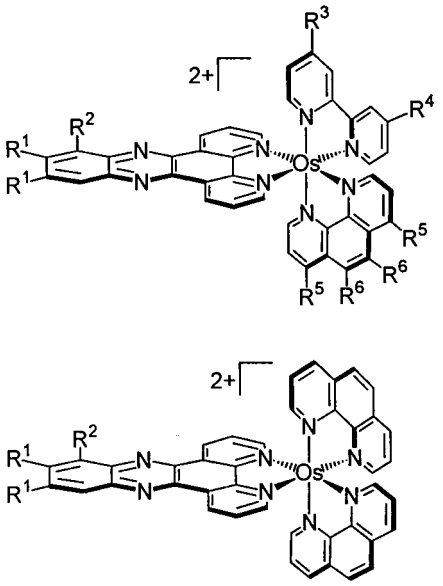

Figure 2. Schematic illustrations of $[Os(phen)_2(dppz)]^{2+}$ derivatives. We developed this family of metallointercalators based on the coordination of three different bidentate, polypyridyl ligands ($L^{1,2,3}$) to the metal center (top; $[Os(L^1)(L^2)(L^3)]^{2+}$), or one intercalating ligand (L^2) and two identical ancillary ligands (L^1) (bottom; $[Os(L^1)_2(R_n\text{-dppz})]^{2+}$). Shown are the Δ enantiomers.

dmp = 4,7-dimethylphen; 5,6-dmp = 5,6-dimethylphen, bpy′ = 4-butyric acid-4-methyl-2,2′-bipyridyl; b′-OMe = 4-butyric acid-4-methyl-2,2′-bipyridyl methyl ester, dab = 4,4′-diamino-2,2′-bipyridyl.

Ion-exchange resins (Sephadex QAE-A25 (anion), SP−C25 (cation)) were obtained from Sigma or Aldrich and preequilibrated in 0.2 M KCl prior to use. Neutral alumina was obtained from Fluka.

Preparation and Isolation of Compounds. 6-Methyldipyrido[3,2-*a*:2′,3′-*c*]phenazine (Me-dppz). 1,10-Phenanthroline-5,6-dione (150 mg; phendione) was dissolved in ethanol (8.6 mL) in a 25-mL round-bottom (RB) flask at 78 °C to give an orange solution. 3-Methyl-1,2-phenylenediamine (260 mg) dissolved in ethanol (3.7 mL) was added slowly to the phendione solution with stirring at 78 °C. After refluxing for 30 min, the dark brown solution was cooled to room temperature, and the product precipitated overnight. The ligand was isolated on a sintered glass frit and washed with cold ethanol, yield 75%. ^{1}H NMR ($CDCl_3$): δ (ppm) 9.70 (m, 2H), 9.40 (d, 2H), 8.20 (d, 1H), 7.85 (m, 4H), 3.05 (s, 3H). FABMS: calcd for $[M + H]^+$ 297.106; found 297.1.

7,8-Dimethyldipyrido[3,2-*a*:2′,3′-*c*]phenazine (Me_2-dppz). Phendione (660 mg) in a 100-mL RB flask was dissolved in ethanol (35 mL) at 78 °C to give an orange solution, and 4,5-dimethyl-1,2-phenylenediamine (807 mg) dissolved in ethanol (14 mL) was added slowly to the solution. Upon addition of the dimethylphenylenediamine, a burst of dark brown was observed, and the Me_2-dppz ligand precipitated as faint yellow needles. The solution was stirred at 78 °C for 5 min and then cooled to room temperature. The precipitate was isolated on a sintered glass frit and washed with excess ethanol, yield 80%. ^{1}H NMR (300 MHz; $CDCl_3$): δ (ppm) 9.63 (dd, J_a = 8 Hz, J_b = 2 Hz, 2H), 9.30 (dd, J_a = 4 Hz, J_b = 2 Hz, 2H), 8.08 (s, 2H), 7.83 (dd, J_a = 8 Hz, J_b = 4, 2H), 2.63 (s, 6H). FABMS: *m*/*z* calcd for $[M + H]^+$ 311; found 311.

4-Methyl-4′-butyric acid methyl ester-2,2′-bipyridyl (bpy′-OMe). Bpy′ (250 mg) was dissolved in methanol (15 mL) in a 250-mL RB flask, and concentrated HCl (15 drops) was added with stirring. The clear solution was heated at reflux for ∼30 min until the starting acid was consumed (TLC (silica): 10:0.95:0.05 CH_2Cl_2/CH_3OH/triethylamine; R_f (bpy′) = 0.1; R_f (bpy′-OMe) = 0.3). The methanol was removed in vacuo, the residue ($[b'\text{-}OMe{\cdot}2H]^{2+}$) was dissolved in water (100 mL), and the pH was raised to 10 with saturated $NaHCO_3$ (aq). The cloudy aqueous solution was extracted with CH_2Cl_2 (3 × 100 mL), and the organic layer was reserved and dried over anhydrous Na_2SO_4. The CH_2Cl_2 was removed in vacuo to give the product in quantitative yield.

$[Os(phen)_2(Me_2\text{-dppz})](PF_6)_2$ and $[Os(L)_2(Me_n\text{-dppz})](PF_6)_2$ Derivatives. $[Os(phen)_2Cl_2]$ (120 mg) and Me_2-dppz (65 mg; 1.1 equiv) were suspended in 16 mL of ethylene glycol (EG) in a 100 mL-RB flask equipped with a magnetic stir bar. The mixture was heated to 160 °C under argon and stirred for 4 h, during which time the starting materials dissolved to give a dark olive green solution. Following the reaction, the solution was cooled to room temperature and filtered. An equivolume portion of NH_4PF_6 (aq; 10% w/v) was added to the EG solution to precipitate the complex as the hexafluorophosphate salt. The dark brown precipitate was isolated on a medium-porosity sintered glass frit and washed extensively with water to remove any soluble impurities and residual EG and with diethyl ether to dry the complex. Purification was achieved on a neutral alumina column using acetonitrile as the eluent. The complex elutes immediately, while unreacted ligand stays on the column. Yield: ∼70%. ^{1}H NMR (300 MHz, CD_3CN): δ (ppm) 9.32 (d, J = 8, 2H), 8.45 (dd, J_a = 7 Hz, J_b = 5 Hz, 4H), 8.30 (s, 4H), 8.21 (d, J = 6 Hz, 2H), 8.17 (s, 2H), 8.04 (d, J = 6 Hz, 2H), 7.98 (dd, J_a = 5 Hz, J_b = 1 Hz, 2H), 7.60 (m, 6H), 2.66 (s, 6H). High-resolution (HR) FABMS: *m*/*z* calcd for $OsC_{44}H_{30}N_8$ ($[M - 2PF_6]$) 862.2215; found 862.2215.

$[Os(phen)_2(Me\text{-}dppz)](PF_6)_2$. ^{1}H NMR (300 MHz, CD_3CN): δ (ppm) 9.63 (d, J = 6 Hz, 1H), 9.57 (d, J = 6 Hz, 1H), 8.55 (m, 4H), 8.40 (s, 4H), 8.25 (m, 2H), 8.19 (m, 2H), 8.10 (m, 4H), 7.85 (m, 2H), 7.75 (m, 4H), 3.10 (s, 3H). HR FABMS: *m*/*z* calcd for $OsC_{43}H_{30}N_8$ $[(M - 2PF_6]^+)$ 848.2059; found 848.2054.

$[Os(5,6\text{-}dmp)_2(Me_2\text{-}dppz)](PF_6)_2$. ^{1}H NMR (300 MHz, CD_2Cl_2): δ (ppm) 9.47 (d, J = 8 Hz, 2H), 8.49 (d, J = 9 Hz, 4H), 8.24 (s, 2H), 8.09 (d, J = 5 Hz, 2H), 8.00 (d, J = 5 Hz, 2H), 7.90 (d, J = 5 Hz, 2H), 7.71 (dd, J_a = 8 Hz, J_b = 6 Hz, 2H), 7.69 (dd, J_a = 8 Hz, J_b = 5 Hz, 2H), 7.67 (dd, J_a = 5 Hz, J_b = 2 Hz, 2H), 2.90 (s, 12H), 2.69 (s, 6H). ESI MS: *m*/*z* calcd for $OsC_{48}H_{38}N_8$ $[(M - 2PF_6]^{2+})$ 459.14; found 459.1 (2+ ion observed; $m = 2(m/z)$).

$[Os(4,7\text{-}dmp)_2(Me_2\text{-}dppz)](PF_6)_2$. ^{1}H NMR (300 MHz, CD_2Cl_2): δ (ppm) 9.43 (d, J = 8 Hz, 2H), 8.38 (s, 4H), 8.24 (s, 2H), 8.07 (d, J = 5 Hz, 2H), 7.97 (d, J = 5 Hz, 2H), 7.83 (d, J = 5 Hz, 2H), 7.74 (dd, J_a = 8 Hz, J_b = 6 Hz, 2H), 7.51 (t, J = 5 Hz, 4H), 3.08 (s, 6H), 3.05 (s, 6H), 2.70 (s, 6H). FABMS: calcd for $[M - PF_6 + H]^+$ 1063.1; found 1063.5. Calcd for $[M - 2PF_6]^+$ 918.3; found 918.2. ESI MS: calcd *m*/*z* for $OsC_{48}H_{38}N_8$ $[(M - 2PF_6]^{2+})$ 459.14; found 459.1 (2+ ion observed; $m = 2(m/z)$).

$[Os(dmob)_2(Me_2\text{-}dppz)](PF_6)_2$. ^{1}H NMR (300 MHz, CD_2Cl_2): δ (ppm) 9.36 (d, J = 8 Hz, 2H), 8.22 (s, 2H), 8.19 (d, J = 5 Hz, 2H), 7.87 (d, J = 3 Hz, 2H), 7.81 (d, J = 3 Hz, 2H), 7.78 (dd, J_a = 8 Hz, J_b = 3 Hz, 2H), 7.60 (d, J = 6 Hz, 2H), 7.32 (d, J = 6 Hz, 2H), 7.09 (dd, J_a = 6 Hz, J_b = 3 Hz, 2H), 6.77 (dd, J_a = 6 Hz, J_b = 3 Hz, 2H), 4.11 (s, 6H), 4.00 (s, 6H), 2.69 (s, 6H). ESI MS: Calcd *m*/*z* for $OsC_{44}H_{38}N_8O_4$ $[(M - 2PF_6]^{2+})$ 467.13; found 467.1 (2+ ion observed; $m = 2(m/z)$).

***cis*-[Os(phen)(Me_2-dppz)Cl_2].** $[Os(phen)Cl_4]$ (500 mg) and Me_2-dppz (300 mg; 0.95 equiv) were suspended in dry DMF (35 mL) in a 100-mL RB flask equipped with a magnetic stir bar. The mixture was heated to reflux under argon and stirred vigorously for ∼4 h (reaction times depend on scale since the reaction involves a suspension). For the first hour, the solution was a dark orange color, consistent with the presence of Os(III). The purple color of the Os(II) was apparent after 2−3 h. Following the reflux, the solution was cooled and filtered on a sintered glass frit. Excess diethyl ether was added to precipitate the product. This material can be used for further reactions; however, it contains trace amounts of Os(III). To characterize the material by ^{1}H NMR, the solid was redissolved in DMF, and an equivolume portion of $Na_2S_2O_4$ (aq) was added dropwise to fully reduce the Os(III) to Os(II) and reprecipitate the product. The dark purple solid was isolated on a medium-porosity sintered glass frit and characterized without further purification. Yield: ∼60%. ^{1}H NMR (300 MHz, CD_2Cl_2): δ (ppm) 10.36 (d, J = 6 Hz, 1H), 10.25 (t, J = 4 Hz, 1H), 9.08 (d, J = 4 Hz, 1H), 8.74 (d, J = 8 Hz, 1H), 8.24 (s, 1H), 8.14 (s, 1H), 8.06 (d, J = 8 Hz, 1H), 7.98 (dd, J_a = 8 Hz, J_b = 6 Hz, 1H), 7.95 (dd, J_a = 4 Hz, J_b = 6 Hz, 1H), 7.96 (s, 2H), 7.88 (d, J = 5 Hz, 1H), 7.79 (d, J = 5 Hz, 1H), 7.62 (d, J = 8 Hz, 1H), 7.02 (dd, J_a = 6 Hz, J_b = 3 Hz, 1H),

7.00 (dd, $J_a = 6$ Hz, $J_b = 3$ Hz, 1H), 2.70 (s, 3H), 2.67 (s, 3H). HR FABMS: *m*/*z* calcd for $[OsC_{22}H_{22}N_2Cl_2]^+$ ($[M]^+$) 752.0905; found 752.0859.

[Os(phen)(bpy′-OMe)(Me$_2$-dppz)](PF$_6$)$_2$ and Derivatives. [Os(phen)(Me$_2$-dppz)Cl$_2$] (200 mg) and bpy′-OMe (75 mg; 1.1 equiv) were suspended in EG (20 mL) in a 100-mL RB flask equipped with a magnetic stir bar. The mixture was heated to 160 °C under argon with stirring for ∼4 h. After 1 h of heating, the dark olive green color of the product can be observed, and it continues to intensify over the course of the reaction. Following the heating period, the solution was cooled to room temperature and filtered on a sintered glass frit. The complex was isolated as the hexafluorophosphate salt as described above. Purification was achieved on neutral alumina, but in contrast to dppz derivatives, bpy′-OMe is eluted from the column with acetonitrile or CH_2Cl_2. Fortunately, the metal complex does not elute off the column with CH_2Cl_2. Therefore, a neutral alumina column was assembled with CH_2Cl_2 as the mobile phase, and the product, dissolved in CH_2Cl_2, was loaded onto the support. The dark band was washed with copious amounts of CH_2Cl_2 to remove unreacted bpy′-OMe, and the desired complex was eluted with acetonitrile. A small amount of purple material ([Os(phen)(Me$_2$-dppz)Cl$_2$]) remained at the top of the column. The acetonitrile solution was evaporated in vacuo to give the desired complex in ∼70% yield. To isolate the complex, the material, after rotary evaporation, was dissolved in a minimal amount of CH_2Cl_2 or acetonitrile, and addition of excess diethyl ether afforded precipitation the complex, which was isolated on a sintered glass frit. ^{1}H NMR (300 MHz, CD_2Cl_2): δ (ppm) 9.53 (d, $J = 9$ Hz, 1H), 9.42 (d, $J = 8$ Hz, 1H), 8.42 (d, $J = 8$ Hz, 1H), 8.32 (d, $J = 8$ Hz, 3H), 8.22 (m, 6H), 8.01 (d, $J = 5$ Hz, 1H), 7.92 (dd, $J_a = 8$, $J_b = 2$ Hz, 1H), 7.88 (m, 2H), 7.64 (m, 3H), 7.44 (m, 1H), 7.16 (d, $J = 7$ Hz, 2H), 3.66 (s, 1.5H), 3.64 (s, 1.5H), 2.96 (t, 2H), 2.69 (s, 9H), 2.46 (t, 2H), 2.04 (q, 2H). HR FAB MS: *m*/*z* Calcd for $OsC_{48}H_{40}N_8O_2$ ($[M - 2PF_6]^+$) 952.2896; found 952.363.

[Os(phen)(dmb)(Me$_2$-dppz)](PF$_6$)$_2$. ^{1}H NMR (300 MHz, CD_2Cl_2): δ (ppm) 9.51 (dd, $J_a = 10$ Hz, $J_b = 1$ Hz, 1H), 9.41 (dd, $J_a = 8$, $J_b = 1$, 1H), 8.41 (dd, $J_a = 8$ Hz, $J_b = 1$ Hz, 1H), 8.2 (m, 9H), 8.01 (dd, $J_a = 5$ Hz, $J_b = 1$ Hz, 1H), 7.93 (dd, $J_a = 8$, $J_b = 5$ Hz, 1H), 7.88 (dd, $J_a = 10$ Hz, $J_b = 4$ Hz, 1H), 7.87 (d, $J = 4$ Hz, 1H), 7.67 (dd, $J_a = 8$ Hz, $J_b = 6$ Hz, 1H), 7.63 (dd, $J_a = 7$ Hz, $J_b = 4$ Hz, 1H), 7.58 (d, $J = 6$ Hz, 1H), 7.40 (d, $J = 6$ Hz, 1H), 7.14 (t, $J = 7$ Hz, 2H), 2.68 (s, 12H). ESI MS: *m*/*z* calcd for $OsC_{44}H_{34}N_8PF_6$ ($[M - PF_6]^+$) 1011.2170; found 1011.2; *m*/*z* calcd for $OsC_{44}H_{34}N_8$ ($[M - 2PF_6]^{2+}$) 433.1264; found 433.1. HR FABMS: *m*/*z* calcd for $OsC_{44}H_{34}N_8$ ($[M - 2PF_6]^+$) 866.2521; found 866.2519.

[Os(phen)(dab)(Me$_2$-dppz)](acetate)$_2$. The complex was prepared from [Os(phen)(Me$_2$-dppz)Cl$_2$] and dab as described above. The hexafluorophosphate salt was exchanged to the chloride salt by anion exchange and purified by HPLC to give the acetate salt (vide infra). ^{1}H NMR (300 MHz, CD_3OD): δ (ppm) 9.44 (d, $J = 8$ Hz, 1H), 9.36 (d, $J = 8$ Hz, 1H), 8.50 (d, $J = 5$ Hz, 1H), 8.43 (m, 2H), 8.32 (m, 5H), 8.09 (d, $J = 5$ Hz, 1H), 7.95 (m, 3H), 7.57 (m, 4H), 7.07 (d, $J = 7$ Hz, 1H), 6.83 (d, $J = 7$ Hz, 1H), 6.47 (dd, $J_a = 6$ Hz, $J_b = 2$ Hz, 1H), 6.42 (dd, $J_a = 6$ Hz, $J_b = 2$ Hz, 1H), 2.73 (s, 3H), 2.71 (s, 3H) (amino protons are exchanged for deuterium in CD_3OD). FABMS calcd for $OsC_{42}H_{31}N_{10}$ [M − 2acetate]+ 867.0; found 867.2.

[Os(phen)(bpy′)(Me$_2$-dppz)](acetate)$_2$. [Os(phen)(Me$_2$-dppz)(bpy′-OMe)](PF$_6$)$_2$ (125 mg) was exchanged to the chloride salt by anion-exchange chromatography (vide infra) and dissolved into 10 mL of H_2O in a 25-mL RB flask equipped with a magnetic stir bar. Aqueous LiOH (1 mL; 1 M) was added to the dark brown/olive solution, and the flask was immersed in an ice bath, with stirring. Stirring was continued overnight as the ice bath warmed to room temperature. The Os(II) solution was diluted to 125 mL with H_2O and neutralized (pH 7) with 1 M HCl. The solution was loaded onto a cation-exchange column (Sephadex SP-C25) that was preequilibrated with KCl. The complex adsorbed to the resin, and the column was washed with several (>2) column volumes of water to remove any uncharged or negatively charged species. The product was eluted from the column in 1:1 H_2O/acetonitrile (100 mM KCl), the solvent was removed in vacuo, and the dry complex was extracted from the salt with CH_2Cl_2. The CH_2Cl_2 was removed in vacuo, and the extraction procedure was repeated to give the dry, salt-free product in quantitative yield. For luminescence studies, the complex was further purified by HPLC (vide infra). ^{1}H NMR (300 MHz, CD_3OD): δ (ppm) 9.58 (dd, $J_a = 4$ Hz, $J_b = 1$ Hz, 1H), 9.47 (d, $J = 8$ Hz, 1H), 8.67 (d, $J = 6$ Hz, 2H), 8.56 (d, $J = 8$ Hz, 1H), 8.47 (d, $J = 8$ Hz, 1H), 8.30 (m, 6H), 8.13 (dd, $J_a = 5$ Hz, $J_b = 3$ Hz, 1H), 7.9 (m, 3H), 7.70 (m, 2H), 7.64 (dd, $J_a = 8$ Hz, $J_b = 5$ Hz, 1H), 7.47 (dd, $J_a = 6$ Hz, $J_b = 4$ Hz, 1H), 2.94 (t, $J = 2$ Hz), 7.20 (m, 2H), 2.73 (s, H), 2.72 (s, 6H), 2.69 (s, 3H), 2.24 (t, $J = 5$ Hz, 2H), 2.00 (q, $J = 8$ Hz, 2H), 1.98 (s, 6H; acetate). ESI MS: *m*/*z* calcd for $OsC_{47}H_{37}N_8O_2$ ($[M - 2acetate - H]^+$) 937.2661; found 937.2; *m*/*z* calcd for $OsC_{47}H_{38}N_8O_2$ ($[M - 2acetate]^{2+}$) 469.1370; found 469.1. HR FABMS: *m*/*z* calcd for $OsC_{47}H_{38}N_8O_2$ ($[M - 2PF_6]^+$) 938.2746; found 938.2746.

For applications in luminescence studies, metal complexes were exchanged to the chloride salt on Sephadex QAE-A25 anion-exchange resin and purified by HPLC (stationary phase, C18 reversed phase; mobile phase, 50 mM ammonium acetate pH 5.5; acetonitrile) to rigorously exclude trace impurities. We found that this procedure always removed luminescent impurities such as tris-phen complexes. The test of purity for the complexes was the absence of emission in aqueous solution.

Enantiomer Resolution. The racemic mixture of [Os(phen)$_2$(dppz)]$^{2+}$ was resolved into its pure Δ and Λ enantiomers by cation-exchange chromatography on Sephadex SP-C25 using potassium bis-tartratodiantimonate (0.15 M) as a chiral eluent. The pure acetate salt of the complex (∼10 mg) was adsorbed onto 5 mL of SP-C25 resin that had been equilibrated for 24 h in 0.2 M KCl (aq) and then washed extensively with H_2O to remove excess salt. The Os(II) coated resin was carefully added to a 1 m × 2.5 cm column of resin to form a symmetric disk approximately 2 cm in height. Approximately 10 cm of free resin was loaded on top of the complex to protect the band during solvent additions. The column was washed with ∼2 L of H_2O, and then the chiral eluent was introduced at a gravity-driven flow rate and the column thoroughly washed with the antimonate solution (∼3 column volumes). The antimonate solution was then recirculated through the column using a peristaltic pump. After 10 days of recirculating the chiral eluent through the column at a gravity-driven flow rate and the complex passing over the column twice, the dark brown band spread into two bands equal in size (5 cm) and color. Resolution was discontinued when the two bands were separated by ∼3 cm of free column support (baseline resolution). The chiral eluent was then washed from the column with several volumes of water, and the stationary phase was pushed out of the column by air pressure while the complex remained adsorbed to the cation-exchange resin. The portions of the resin that contained each enantiomer were excised, and each isomer was eluted from the resin with KCl (50 mM) in acetonitrile/water (1:1). Upon removing the solvent in vacuo, the complex was extracted from the salt into CH_2Cl_2. The CH_2Cl_2 was removed in vacuo to give the dry, salt-free enantiomer. Circular dichroism (CD) spectra (Supporting Information) were recorded on a Jasco J-500A, and data for the complexes are as follows: for Δ-[Os(phen)$_2$(dppz)]$^{2+}$, $\Delta\epsilon$ (270 nm) = −209 M^{-1} cm^{-1}; and for Λ-[Os(phen)$_2$(dppz)]$^{2+}$, $\Delta\epsilon$ (270 nm) = +214 M^{-1} cm^{-1}.

Methods. UV−vis. Extinction coefficients were determined by measuring the mass of three samples of complex that had been dried in vacuo for 48 h, preparing 10-mL solutions of each sample, and measuring the absorbance at the appropriate wavelength. Individual scans were measured on a Beckman DU-7400 diode array spectrophotometer. Titrations were carried out on a Cary 2200, double-beam spectrophotometer. To begin, the sample cuvette contained the Os(II) complex in standard buffer (vide supra), and the reference cuvette contained only buffer. A concentrated (∼15−20 mM nucleotides) aliquot (1−10 μL) of buffered DNA solution was added to each cuvette, and the solutions were mixed by bubbling air into the cuvette with a micropipet equipped with a plastic tip for ∼30 s. The absorbance of the sample solution was recorded against the DNA-containing reference. The percent hypochromism was calculated as % hyp = $[(A_\lambda^{[DNA]=0} - A_\lambda^{[DNA]=N})/A_\lambda^{[DNA]=0}] \times 100$.

Luminescence Measurements. All samples were air equilibrated. Steady-state emission data were recorded on an SLM-8000 spectrofluorimeter. Emission intensities were determined by integration of the

Scheme 1. Synthesis of Dipyridophenazine Derivatives[a]

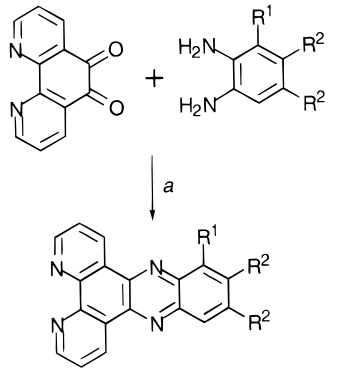

[a] Reagents and conditions: (a) EtOH, reflux, 5 min.[21]

luminescence spectrum and standardized against $[Ru(bpy)_3]^{2+}$ as a calibration for the instrument. Spectra were not corrected for instrument sensitivity owing to their near-infrared emission. Therefore, emission yields represent a minimum absolute value, but relative values are accurate and valid. Quantum yields for emission were determined as described previously by comparison to known standards such as $[Ru(bpy)_3]^{2+}$ and $[Os(bpy)_3]^{2+}$.

Luminescence lifetimes were measured by time-correlated single photon counting (TCSPC) and multifrequency phase-modulation fluorometry (MPMF). TCSPC data were collected and analyzed as described previously.[4] MPMF data were collected on an ISS K2 lifetime fluorometer according to ISS protocol over frequency ranges dictated by the lifetime of the sample.[23] Typical frequency ranges spanned 0.1−150 MHz, and data were collected at a minimum of 10 frequencies (5−7 measurements per frequency). Data analysis was achieved on commercial software (ISS), and the quality of the model was judged by the value of χ^2 for the least-squares minimization. Simulations with $\chi^2 < 10$ were accepted as good fits.

Electrochemical Measurements. Reduction potentials were measured by cyclic voltammetry (CV) using instrumentation described previously.[4] Complexes were dissolved in dry DMF (Fluka; stored over molecular sieves) containing 0.1 M tetrabutylammonium hexafluorophosphate as the supporting electrolyte. Electrochemical windows ranging from 0.2 to 1.6 V vs NHE for oxidation and 0.2 to −1.55 V vs NHE for reduction were scanned at a rate of 0.1 V/s. $E_{1/2}$ values were taken as the average of the voltage of maximum current for the forward and reverse electrochemical processes.

Results

Synthesis. Preparation of Ligands. The preparation of polypyridyl ligands for coordination to metal centers has been described extensively in the literature.[20,24] In this study, we took advantage of commercially available bpy and phen derivatives and made simple modifications to these parent compounds where necessary using methods described previously.[20,24]

The synthesis of the dppz derivatives for application as intercalating ligands followed the procedure described by Dickeson and co-workers,[21] with slight modification. In this approach, the dppz derivative is obtained by condensation of the appropriately substituted o-diaminobenzene with 5,6-phenanthroline-5,6-dione in boiling ethanol (Scheme 1).

Preparation of Metal Complexes. In general, the compounds prepared for this study can be divided into two classes: $[Os(L^1)_2(L^2)]^{2+}$ and $[Os(L^1)(L^2)(L^3)]^{2+}$ where L^1 and L^+ are derivatives of phen or bpy and L^2 is a derivative of dppz. For the $[Os(L^1)_2(L^2)]^{2+}$ class, the complexes are prepared by

Scheme 2. Synthesis of $[Os(phen)(bpy')(Me_2\text{-dppz})]^{2+}$ [a,b]

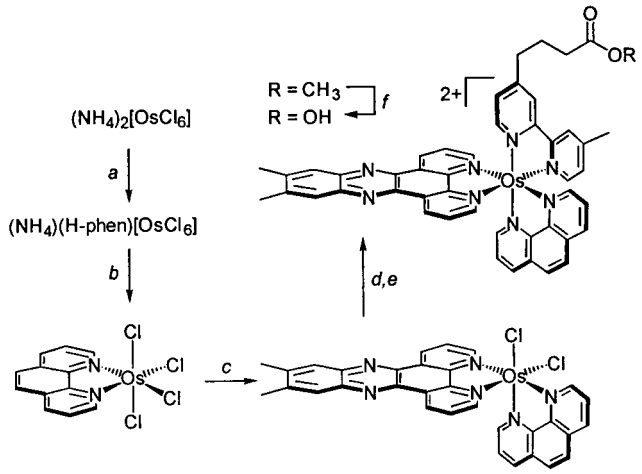

[a] Reagents and conditions: (a) phen (1 equiv), 3 N HCl (aq);[22] (b) solid-state pyrolysis, 290 °C, molten $KNO_3/NaNO_3$ (1:9), 8 h;[22] (c) Me_2-dppz (0.9 equiv), DMF, reflux, 4 h; (d) b′-OMe, ethylene glycol, 160 °C, 3 h; (e) 10% NH_4PF_6 (aq), metathesis to dichloride salt by anion exchange; (f) LiOH (aq; 10 equiv), 25 °C, 12 h.

coordination of the dppz derivative to an $[Os(L^1)_2Cl_2]$ precursor, using well-established methods for the synthesis of mixed-ligand complexes of Os(II).[25,26]

To our knowledge, only one method to obtain complexes of the $[Os(L^1)(L^2)(L^3)]^{2+}$ type, so-called tris heteroleptic complexes of Os(II), has been described.[28] This approach, which appeared after we began our work, is fairly laborious and requires several steps. Scheme 2 outlines the procedure we use to synthesize polypyridyl complexes of Os(II) that contain three different bidentate polypyridyl ligands. The key intermediate in this approach is $[Os(phen)Cl_4]$, which is obtained in high yield by solid-phase pyrolysis as described by Meyer and co-workers.[22]

With $[Os(phen)Cl_4]$ in hand, a second polypyridyl ligand may be introduced by refluxing the tetrachloro complex and 1 equiv of the desired ligand in DMF. The product contains a mixture of Os(II) and Os(III) oxidation states (as evident in ^{1}H NMR spectra). To convert all of the Os(III) to Os(II), the Os(III) is reduced by aqueous sodium dithionite.

Introduction of the third bidentate ligand follows from protocols established for the preparation of $[Os(L^1)_2(L^2)]^{2+}$ complexes.[22,25] In our procedure, the $[Os(phen)(L^2)Cl_2]$ complex and the appropriate polypyridyl ligand (L^3) are heated in ethylene glycol. Over the course of the reaction, L^3 dissolves and the solution turns to a characteristic olive green color, consistent with the presence of a tris(polypyridyl) Os(II) complex. Alternative solvents such as 1:1 water/ethanol (refluxing) may be used if sensitive functionalities are present on L^3; however, these conditions require as much as 48 h of reflux. The desired complex, $[Os(phen)(L^2)(L^3)]^{2+}$, is isolated by precipitation as the $^-PF_6$ salt.

Characterization. Structural Assessment by ^{1}H NMR and Mass Spectrometry. We employed several analytical methods to characterize the materials synthesized in these studies including ^{1}H NMR, mass spectrometry, ultraviolet−visible (UV−vis) spectroscopy, and cyclic voltammetry. The two

(23) Vandeven, M.; Barbieri, B.; Gratton, E. *Biophys. J.* **1993**, *64*, a221−a221.
(24) Nazeeruddin, M. K.; Zakeeruddin, S. M.; Kalyanasundaram, K. *J. Phys. Chem.* **1993**, *97*, 9607−9612.
(25) Buckingham, D. A.; Dwyer, F. P.; Sargeson, A. M. *Aust. J. Chem.* **1964**, *17*, 622−631.
(26) Buckingham, D. A.; Dwyer, F. P.; Goodwin, H. A.; Sargeson, A. M. *Aust. J. Chem.* **1964**, *17*, 315−324.
(27) Buckingham, D. A.; Dwyer, F. P.; Goodwin, H. A.; Sargeson, A. M. *Aust. J. Chem.* **1964**, *17*, 325−336.
(28) Jandrasics, E. Z.; Keene, F. R. *J. Chem. Soc., Dalton Trans.* **1997**, 2.

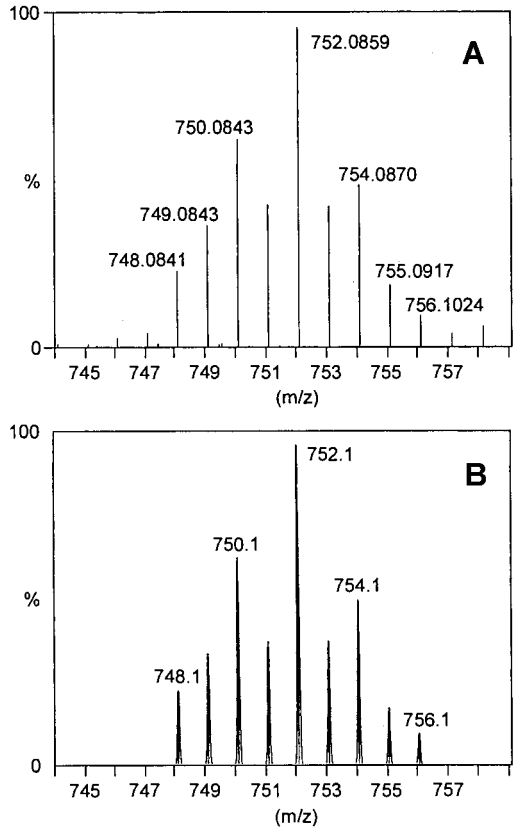

Figure 3. (A) Observed spectrum for the analysis of $[Os(phen)(Me_2\text{-}dppz)Cl_2]$ by high-resolution fast-atom-bombardment mass spectrometry. (B) Calculated isotopic distribution for the molecular ion $[OsC_{22}H_{22}N_2Cl_2]^+$. The agreement of the observed and calculated masses and isotopic patterns confirms the composition of the complex.

simplest and most useful structural tools are ^{1}H NMR and mass spectrometry.

The ^{1}H NMR spectrum of $[Os(phen)(Me_2\text{-}dppz)(bpy')]^{2+}$ (Supporting Information) contains several overlapping resonances in the aromatic region, owing to the significant number of unique protons in this complex. Fortunately, well-defined resonances at 10.5 and 10.9 ppm, which correspond to protons at the 4- and 7-positions of the phenanthroline moiety of the dppz derivative, can be used to confirm the identity of the complex in this spectrum. The spectrum at 300 MHz shows a broad singlet in the aliphatic region, which accounts for all three of the methyl groups (two on Me_2-dppz, one on bpy′). Owing to the asymmetry of this ligand, the complex is present as two diastereomers: one where the butyric acid is oriented in an axial direction relative to the Me_2-dppz plane and one where the group is equatorial. The presence of these two isomers is apparent only in the aliphatic region of the NMR spectrum of this compound, which is expected, since the differences in the isomers are significant only for a substituent that extends away from the metal center.

^{1}H NMR data alone are not sufficient to establish the structure of a complex with three different polypyridyl ligands. One can imagine that, over the course of the synthesis of an $[Os(L^1)(L^2)(L^3)]^{2+}$ complex, one obtains only a statistical mixture of complexes with varying degrees of ligand diversity about the metal center.

A high-resolution (HR) FABMS of $[Os(phen)(Me_2\text{-}dppz)Cl_2]$ is shown in Figure 3, and a comprehensive summary of the analysis by MS of the family of metallointercalators based on Os(II) is listed in Table 1. For the data in Figure 3, we find no signals at *m*/*z* values that correspond to $[Os(phen)_2Cl_2]$ or $[Os(Me_2\text{-}dppz)_2Cl_2]$. Thus, it is unlikely that any scrambling of the polypyridyl ligands occurs during the synthesis. The HR data in Figure 3A (observed) and Figure 3B (calculated) provide an unambiguous confirmation of the identity of the material and validate our method of introducing one Me_2-dppz ligand onto the metal center.

Also shown in Table 1 are the MS data for several $[Os(L^1)_2(L^2)]^{2+}$ and $[Os(L^1)(L^2)(L^3)]^{2+}$ complexes. These data establish the efficacy of our methods to introduce a third polypyridyl ligand onto $[Os(phen)(Me_2\text{-}dppz)Cl_2]$ to give complexes with three different bidentate, polypyridyl ligands without generating statistical mixtures of homoleptic complexes.

Visible Absorption Spectroscopy. Polypyridyl complexes of Os(II) are characterized by intense absorption into metal-to-ligand charge-transfer (MLCT) excited states in the visible region of the electromagnetic spectrum.[29,30] Figure 4 shows the absorption spectra of Me_2-dppz, $[Os(phen)_3]^{2+}$, and $[Os(phen)_2(Me_2\text{-}dppz)]^{2+}$. The near-visible absorption of Me_2-dppz consists of a $\pi-\pi^*$ transition centered on the phenazine portion of the polypyridyl ligand. The absorption profile of $[Os(phen)_3]^{2+}$ is dominated by transitions into the ^{1}MLCT (400−480 nm) states as well as formally spin forbidden transitions into the ^{3}MLCT states (580−725 nm). On the basis of Figure 4, the spectrum of $[Os(phen)_2(Me_2\text{-}dppz)]^{2+}$ consists of the sum of two spectral components: the absorption of Me_2-dppz together with that of $[Os(phen)_3]^{2+}$. It is noteworthy that the spectrum of $[Os(phen)_2(Me_2\text{-}dppz)]^{2+}$ reflects lower extinction coefficients for each of the chromophores when compared with coefficients for the individual species.

Figure 5 compares the absorption spectra for $[Os(phen)_2(dppz)]^{2+}$ and $[Ru(phen)_2(dppz)]^{2+}$. Each complex displays visible absorption; however, the absorption by the osmium complex extends out beyond 700 nm, while the absorption by ruthenium is not significant at wavelengths longer than ∼550−600 nm. The low-energy absorption by the osmium complex is the result of direct excitation into ^{3}MLCT states.[29,30] This transition is spin-forbidden for both complexes, however, and therefore is not observed with ruthenium. With osmium, spin−orbit coupling results in mixing of the ^{1}MLCT and ^{3}MLCT states. This mixing gives the triplet state some singlet character and allows for the transition to occur. As a result of absorption across the entire visible region of the spectrum, dppz complexes of Os(II) and polypyridyl complexes of Os(II) in general are darkly colored and appear almost black in concentrated solution.

The transition at 374 nm is centered on the dppz ligand.[9] The energy of this absorption does not change upon substitution of the metal center. This observation suggests that there is very little electronic coupling between the metal center and the phenazine portion of the molecule.

It is also noteworthy that the lowest energy ^{1}MLCT transition occurs at lower energy for osmium than for ruthenium. This observation is consistent with the $5d^6$ ground-state configuration of Os(II), which commands a lower third ionization potential compared with Ru(II).[22,29]

Table 2 lists the wavelength of maximum absorption (λ_{max}) for the $\pi-\pi^*$ transition centered on the dppz derivative, and the λ_{max} for lowest energy ^{1}MLCT transition for the series of compounds employed in this study. Across this series, the incorporation of substituents on the phenazine portion of the dppz derivative perturbs the $\pi-\pi^*$ transition on this ligand but

(29) Creutz, C.; Chou, M.; Netzel, T. L.; Okumura, M.; Sutin, N. *J. Am. Chem. Soc.* **1980**, *102*, 1309−1319.
(30) Kober, E. M.; Meyer, T. J. *Inorg. Chem.* **1984**, *23*, 3877−3886.

Table 1. Mass Spectrometry Results for $[Os(phen)_2(dppz)]^{2+}$ Derivatives

complex[a]	ion[b]	formula	calcd mass	obsd (m/z)[c]	method[d]
$[Os(phen)(Me_2\text{-dppz})Cl_2]$	$[M]^+$	$OsC_{32}H_{22}N_6Cl_2$	752.0905	752.0859	HR FAB
$[Os(phen)_2(dppz)]^{2+}$	$[M]^+$	$OsC_{42}H_{26}N_8$	834.1902	834	FAB
$[Os(phen)_2(Me\text{-dppz})]^{2+}$	$[M]^+$	$OsC_{43}H_{28}N_8$	848.2052	848.2054	HR FAB
$[Os(phen)_2(Me_2\text{-dppz})]^{2+}$	$[M]^+$	$OsC_{44}H_{30}N_8$	862.2215	862.2208	HR FAB
$[Os(4,7\text{-dmp})_2(Me_2\text{-dppz})]^{2+}$	$[M]^{2+}$	$OsC_{48}H_{38}N_8$	918.2841	459.2	ESI
$[Os(5,6\text{-dmp})_2(Me_2\text{-dppz})]^{2+}$	$[M]^{2+}$	$OsC_{48}H_{38}N_8$	918.2841	459.1	ESI
$[Os(dmob)_2(Me_2\text{-dppz})]^{2+}$	$[M]^{2+}$	$OsC_{44}H_{38}N_8O_4$	934.2638	467.1	ESI
$[Os(phen)(dmb)(Me_2\text{-dppz})]^{2+}$	$[M]^+$	$OsC_{44}H_{34}N_8$	866.2521	866.2519	HR FAB
$[Os(phen)(bpy')(Me_2\text{-dppz})]^{2+}$	$[M]^+$	$OsC_{47}H_{38}N_8O_2$	938.2746	938.2746	HR FAB
$[Os(phen)(b'\text{-OMe})(Me_2\text{-dppz})]^{2+}$	$[M]^+$	$OsC_{48}H_{40}N_8O_2$	952.2896	952.363	ESI
$[Os(phen)(dab)(Me_2\text{-dppz})]^{2+}$	$[M-H]^+$	$OsC_{42}H_{31}N_{10}$	867.2355	867.2	FAB

[a] Me_2-dppz = 7,8-dimethyldipyridophenazine; Me-dppz = 6-methyldipyridophenazine; dmob = 4,4′-dimethoxy-2,2′-bipyridyl; 4,7-dmp = 4,7-dimethylphen; 5,6-dmp = 5,6-dimethylphen, bpy′ = 4-butyric acid-4-methyl-2,2′-bipyridyl; b′-OMe = 4-butyric acid-4-methyl-2,2′-bipyridyl methyl ester, dab = 4,4′-diamino-2,2′-bipyridyl. [b] For $[M]^+$ ions, the 2+ complex is reduced by the matrix to give a singly charged ion. [c] The mass of the complex is the product of the charge of the ion and the mass-to-charge ratio (m/z). For $[M]^{2+}$ ions, $m = 2(m/z)$. [d] FAB = fast atom bombardment; ESI = electrospray ionization; HR = high resolution.

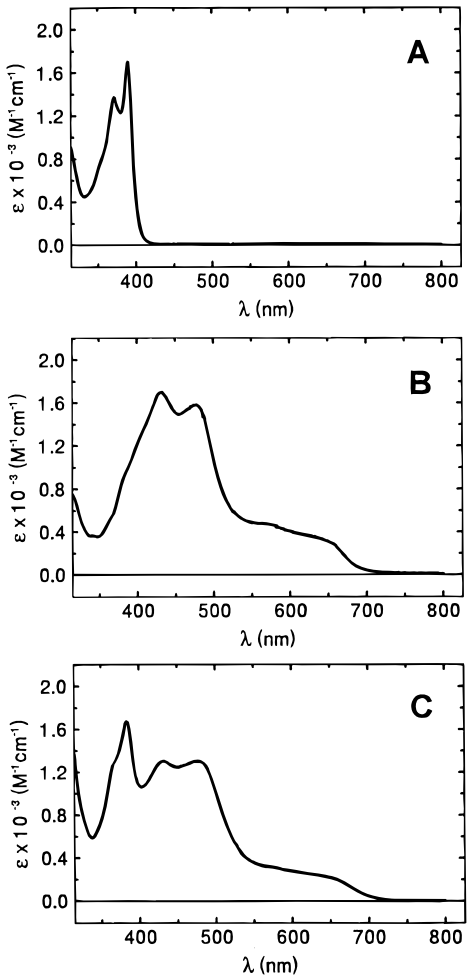

Figure 4. Visible absorption spectra of (A) Me_2-dppz in 10:1 water/acetonitrile; (B) $[Os(phen)_3]^{2+}$ in water; and (C) $[Os(phen)_2(Me_2\text{-dppz})]^{2+}$ in water.

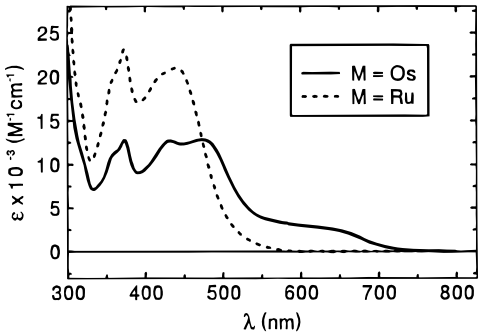

Figure 5. Comparison of the visible absorption spectra for $[M(phen)_2(dppz)]^{2+}$ complexes in water.

Table 2. Visible Absorption Properties for $[Os(phen)_2(dppz)]^{2+}$ Derivatives in Aqueous Solution

	λ_{max} nm ($\epsilon \times 10^{-4}$)	
complex[a]	$\pi-\pi^*$ on R_n-dppz[b,c]	^{1}MLCT[b,d]
$[Os(phen)_2(dppz)]^{2+}$	374 (1.27)	473 (1.30)
$[Os(phen)_2(Me\text{-dppz})]^{2+}$	374 (1.15)	475 (1.32)
$[Os(phen)_2(Me_2\text{-dppz})]^{2+}$	384 (1.68)	475 (1.30)
$[Os(4,7\text{-dmp})_2(Me_2\text{-dppz})]^{2+}$	384 (1.52)	477 (1.23)
$[Os(5,6\text{-dmp})_2(Me_2\text{-dppz})]^{2+}$	384 (1.69)	475 (1.34)
$[Os(dmob)_2(Me_2\text{-dppz})]^{2+}$	384 (1.84)	485 (1.20)
$[Os(phen)(bpy')(Me_2\text{-dppz})]^{2+}$	384 (1.87)	479 (1.39)
$[Os(phen)_3]^{2+}$		477 (1.58)
Me_2-dppz[e]	389 (1.7)	

[a] See Table 1 for explanation of ligand abbreviations. [b] Uncertainties in λ_{max} and ϵ are ±4 nm and ±10%, respectively. [c] For Me_2-dppz, $n = 2$; R = CH_3. For Me-dppz, $n = 1$; R = CH_3. For dppz R = H. [d] The ^{1}MLCT transition has two discernible maxima. The data listed are for the lowest energy transition. [e] For solubility considerations, data were recorded in a mixture of acetonitrile and water.

does not affect the MLCT transitions. Conversely, substituents on the ancillary phen or bpy derivatives affect only the MLCT transitions but not the absorption centered on the dppz derivative.

Redox Properties. We employed cyclic voltammetry to measure the relevant reduction and oxidation properties for the family of osmium complexes. Panels A and B of Figure 6 show an oxidation wave and a reduction wave, respectively, for $[Os(phen)_2(Me_2\text{-dppz})]^{2+}$ in DMF. Scheme 3A,B illustrates the oxidation and reduction processes that account for the flow of current detected in each experiment. Consistent with previous studies of polypyridyl complexes of Os(II),[22] oxidation is metal-centered and corresponds to the Os(III)/Os(II) couple. The observed reductions are ligand-centered and correspond to one-electron reductions first on the phenazine portion of the Me_2-dppz ligand and then each of the two phenanthrolines.

Table 3 shows the reduction potentials for the metal-centered and ligand-centered processes for the entire family of complexes. As expected, the incorporation of electron-donating methyl groups on the 6- or 7- and 8-positions of the dppz derivatives shifts the phenazine-centered reduction toward the negative, corresponding to a higher energy for reduction. Each methyl group shifts the potential ~ -50 mV. These substituents do not affect the potential of the metal-centered couple.

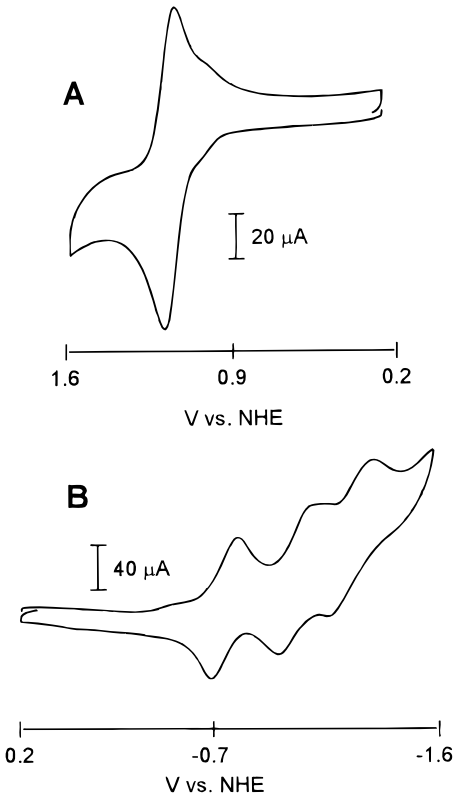

Figure 6. Cyclic voltammograms for the oxidation (A) and reduction (B) of $[Os(phen)_2(Me_2\text{-}dppz)](PF_6)_2$ in DMF. The relevant redox properties are outlined in Scheme 3. See Table 3 for conditions.

The incorporation of electron-donating substituents on the ancillary phen or bpy ligands shifts the Os(III)/Os(II) reduction to the negative as well. These data are consistent with the electron donors stabilizing the Os(III) state via raising the absolute energy of the highest occupied molecular orbital (HOMO).[31]

In summary, the redox chemistry of dppz complexes of Os(II) is a superposition of two redox-active components. The metal-centered (3+/2+) couple can be manipulated by incorporating electron-donating or -withdrawing substituents on the ancillary ligands, without affecting the ligand-centered reduction. Substituents on the phenazine portion of the dppz ligand affect the phenazine reduction potential but not the metal-centered potential.

Photophysical Studies. Probing DNA Binding with Visible Absorption Spectroscopy. We followed the association of the dppz complexes of Os(II) with double-helical DNA by absorption spectroscopy. Owing to the well resolved $\pi-\pi^*$ transition on the phenazine portion of the dppz derivative in these complexes, one can delineate processes that are localized on this ligand.

The binding of $[Ru(phen)_2(dppz)]^{2+}$ and $[Os(phen)_2(dppz)]^{2+}$ to DNA occurs by preferential intercalation of the dppz ligand into the hydrophobic interior of the DNA base stack and is accompanied by significant hypochromism in the $\pi-\pi^*$ transition on the intercalating ligand.[3,32] Figure 7 shows absorption spectra of $[Os(phen)_2(Me_2\text{-}dppz)]^{2+}$ in the presence of increasing concentrations of mixed-sequence CT DNA, poly d(AT), and poly d(GC). Like its parent complex, the association of $[Os(phen)_2(Me_2\text{-}dppz)]^{2+}$ with DNA results in a significant perturbation in the $\pi-\pi^*$ transition on Me_2-dppz, consistent with preferential intercalation of this ligand into the base stack of the DNA helix.

Scheme 3. Summary of the Metal-Centered (A) and Ligand-Centered (B) Redox Processes for $[Os(phen)_2(Me_2\text{-}dppz)]^{2+}$ Measured by Cyclic Voltammetry (Figure 6)[a]

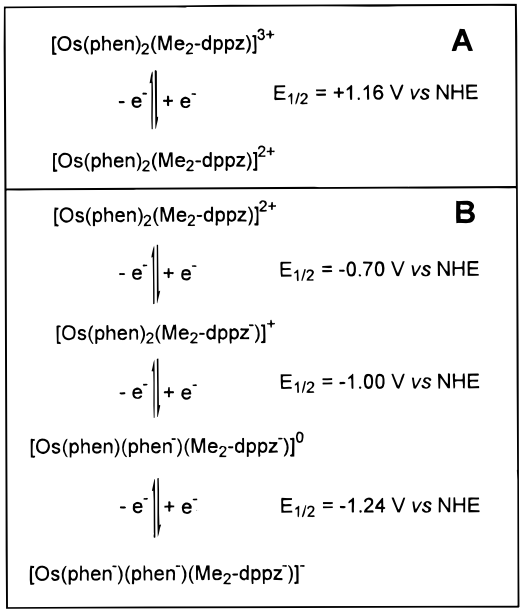

[a] See Table 3 for conditions.

A plot of percent hypochromism versus the ratio of nucleotides to osmium ($R_{nuc:Os}$) is shown in Figure 8. With increasing DNA concentration, the percent hypochromism increases linearly until reaching saturation at $R_{nuc:Os} = \sim 5$. For $R_{nuc:Os}$ values of ~100:1, the percent hypochromism actually decreases slightly. Simple fits of these plots indicate binding constants (K_B) with a lower limit of $\sim 10^6$ M^{-1}; however, these experiments require concentrations that are several orders of magnitude higher than K_B. Therefore, these data are not sufficient to establish K_B values with acceptable accuracy.

It is useful to compare the percent hypochromism in the $\pi-\pi^*$ transition on the dppz derivative for the entire series of Os(II) intercalators in the presence of DNA polymers at saturation (Table 4). Across this series, significant hypochromism, which depends on the ligand architectures of the metallointercalators, is observed. For example, complexes with substituents on the 4-position of the phen or bpy ancillary ligand generally exhibit less hypochromism than do complexes with hydrogen in this position. These different amounts of hypochromism likely reflect different levels of penetration of the dppz ligand into the DNA base stack, although different K_B values may also contribute to the ligand-dependent hypochromism.

Luminescence Studies in the Presence and Absence of DNA. (A) Luminescence in Dichloromethane. Luminescence from dppz complexes of transition metals such as Ru(II), Os(II), and Re(I) is remarkably sensitive to water, owing to quenching by proton transfer to the phenazine nitrogens of the photoexcited complex.[3,5−8,13] To measure the inherent quantum yields for emission (Φ_{em}) for each of the osmium complexes without interference by water-induced quenching, we sought to study their luminescence profiles in a nonaqueous solvent. Therefore, we chose CH_2Cl_2 as a suitable nonaqueous, aprotic solvent that could be rigorously dried.

(31) (a) Kober, E. M.; Caspar, J. V.; Lumpkin, R. S.; Meyer, T. J. *J. Phys. Chem.* **1986**, *90*, 3722−34. (b) Schoonover, J. R.; Bates, W. D.; Meyer, T. J. *Inorg. Chem.* **1995**, *34*, 6421−6422.

(32) Hiort, C.; Lincoln, P.; Nordén, B. *J. Am. Chem. Soc.* **1993**, *115*, 3448−3454.

Table 3. Ground-State Reduction and Excited-State Oxidation Potentials for $[Os(phen)_2(dppz)]^{2+}$ Derivatives

	metal centered[b,c]		ligand centered[b,c]		
complex[a]	(*2+/3+)[d]	(3+/2+)	dppz/dppz−	L2/L2−	L3/L3−
$[Os(phen)_2(dppz)]^{2+}$	0.76	1.16	−0.61	−0.98	−1.21
$[Os(phen)_2(Me\text{-}dppz)]^{2+}$	0.73	1.19	−0.66	−1.00	−1.23
$[Os(phen)_2(Me_2\text{-}dppz)]^{2+}$	0.76	1.16	−0.70	−1.00	−1.24
$[Os(4,7\text{-}dmp)_2(Me_2\text{-}dppz)]^{2+}$	0.89	1.03	−0.74	−1.17	−1.38
$[Os(5,6\text{-}dmp)_2(Me_2\text{-}dppz)]^{2+}$	0.81	1.11	−0.72	−1.06	−1.30
$[Os(dmob)_2(Me_2\text{-}dppz)]^{2+}$	0.87	0.90	−0.75	−1.16	−1.36
$[Os(phen)(dmb)(Me_2\text{-}dppz)]^{2+}$	0.81	1.11	−0.70	−1.04	−1.32
$[Os(phen)(dab)(Me_2\text{-}dppz)]^{2+}$		0.86	−0.71	−1.08	−1.39
$[Os(Me_2\text{-}dppz)_3]^{2+}$		1.01	−0.74	−1.00	

[a] See Table 1 for explanation of ligand abbreviations. [b] Potentials are reported in volts vs NHE, and uncertainty is estimated to be ±50 mV. [c] Measured against Ag/AgCl (3 M KCl) at a glassy carbon working electrode in dry DMF at a scan rate of 0.1 $V \cdot s^{-1}$. The supporting electrolyte was 0.1 M tetrabutylammonium hexafluorophosphate, and the auxiliary electrode was Pt wire. [d] Excited-state oxidation potential taken as the difference between the highest energy point along the emission spectrum (~1.92 eV) and the 3+/2+ reduction potential.

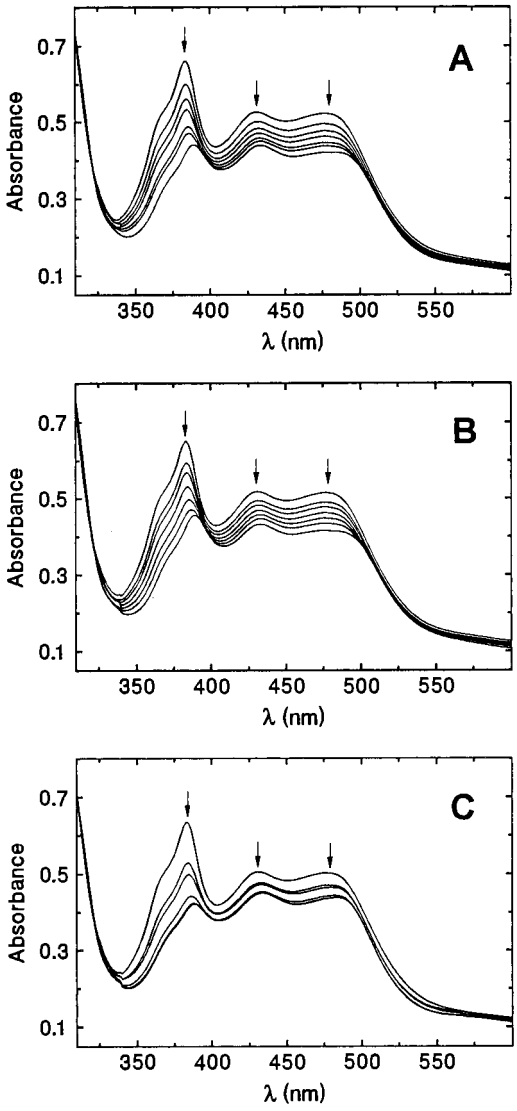

Figure 7. Visible absorption spectra of aqueous $[Os(phen)_2(Me_2\text{-}dppz)]^{2+}$ as a function of increasing concentrations of (A) mixed-sequence (CT) DNA; (B) poly d(AT); and (C) poly d(GC). Conditions were as follows: [Os] = 30 μM; [DNA] = 0−0.6 mM nucleotides in 5 mM Tris, 50 mM NaCl, pH 8.5.

We measured the excited-state lifetime by two time-resolved emission techniques: single photon counting (SPC)[4] and multifrequency phase-modulation fluorometry (MPMF).[23] Results obtained from data collected by both techniques were identical. We also measured the excited-state lifetimes of well-studied

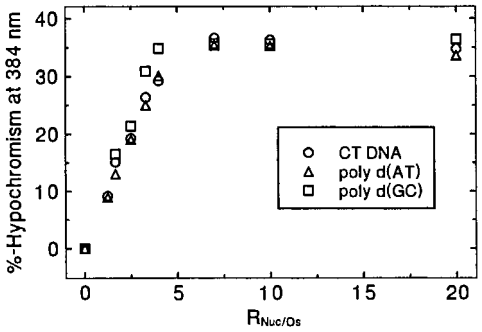

Figure 8. Percent hypochromism at 384 nm for $[Os(phen)_2(Me_2\text{-}dppz)]^{2+}$ in the presence of increasing amounts of duplex DNA (see figure legend). Conditions are described in Figure 7 caption.

Table 4. Hypochromism Observed for Association of Dipyridophenazine Complexes of Os(II) with DNA by Intercalation

	% hypochromism[a]		
complex[b]	CT[c]	poly d(AT)[c]	poly d(GC)[c]
$[Os(phen)_2(dppz)]^{2+}$	31.3	31.5	34.9
$[Os(phen)_2(Me\text{-}dppz)]^{2+}$	26.6	31.1	32.8
$[Os(phen)_2(Me_2\text{-}dppz)]^{2+}$	31.0	33.0	34.8
$[Os(4,7\text{-}dmp)_2(Me_2\text{-}dppz)]^{2+}$	26.7	33.9	35.4
$[Os(5,6\text{-}dmp)_2(Me_2\text{-}dppz)]^{2+}$	30.8	32.4	37.1
$[Os(dmob)_2(Me_2\text{-}dppz)]^{2+}$	32.8	33.9	33.6
$[Os(phen)(b'\text{-}OMe)(Me_2\text{-}dppz)]^{2+}$	25.8	27.5	28.7
$[Os(phen)(bpy')(Me_2\text{-}dppz)]^{2+}$	27.5	30.9	30.7

[a] % hypochromism = 100 × [[*A*(DNA = 0) − *A*(DNA = 1 mM nucleotides)]/*A*(DNA = 0)]. Values are for M/DNA = 1:50 bp. Uncertainties are ±0.1 (% hypochromism). [b] See Table 1 for explanation of ligand abbreviations. [c] Conditions: [Os] = 10 μM, [DNA] = 1 mM nucleotides in buffer (5 mM Tris, 50 mM NaCl, pH 8.5).

complexes such as $[Os(bpy)_3]^{2+}$ and found that either technique gave results that matched values reported previously.[29] The MPMF technique is remarkably simple and allows one to collect and analyze several data sets in the time required for a single data collection run by SPC.

The excited-state lifetimes for several polypyridyl complexes of Os(II) in CH_2Cl_2 solution are listed in Table 5. Across this series of complexes, all of the time-resolved emission decays are strictly monoexponential. The observation of single exponential decays for the complexes in a nonaqueous solvent is important because, in the presence of DNA, the emission profiles are considerably more complex. Thus, we may conclude that the complexity of the luminescence decays with DNA is not the result of impure osmium samples.

The Φ_{em} values for each complex in Table 5 are also listed. Φ_{em} was determined by comparing the steady-state emission

Table 5. Monoexponential Luminescence Lifetimes and Quantum Yields for Emission for Osmium Complexes in Dichloromethane

complex[a]	τ (ns)[b]	Φem[b,c] $\times 10^3$
$[Os(phen)_2(dppz)]^{2+}$	50.4	4.2
$[Os(phen)_2(Me\text{-}dppz)]^{2+}$	62.0	5.2
$[Os(phen)_2(Me_2\text{-}dppz)]^{2+}$	73.8	6.2
$[Os(4,7\text{-}dmp)_2(Me_2\text{-}dppz)]^{2+}$	43.0	3.6
$[Os(5,6\text{-}dmp)_2(Me_2\text{-}dppz)]^{2+}$	63.2	5.3
$[Os(dmob)_2(Me_2\text{-}dppz)]^{2+}$	13.4	1.1
$[Os(phen)(dmb)(Me_2\text{-}dppz)]^{2+}$	85.2	7.1
$[Os(bpy)_3]^{2+}$	69.0	5.8
$[Os(phen)_3]^{2+}$	143.4	13.3

[a] See Table 1 for explanation of ligand abbreviations. [b] Error is ±10%. [c] Quantum yields for emission (Φ_{em}) determined by comparison to $[Os(bpy)_3]^{2+}$ in acetonitrile.[30]

yield and the excited-state lifetime of each complex to that of $[Os(bpy)_3]^{2+}$ in acetonitrile and CH_2Cl_2.

Several general observations with respect to Φ_{em} can be made from Table 5. First, the emission yield for each complex is within a factor of 1.5 of that for $[Os(bpy)_3]^{2+}$ in CH_2Cl_2. This observation parallels the fact that the emission yield of $[Ru(phen)_2(dppz)]^{2+}$ resembles that of $[Ru(bpy)_3]^{2+}$. Second, it is apparent that the incorporation of methyl groups on the phenazine portion of the dppz derivative leads to an increase in Φ_{em} going from dppz to Me-dppz to Me_2-dppz.

For the series of complexes containing one Me_2-dppz ligand and either two phen derivatives or one phen and a bpy derivative, the emission yields decrease when electron-donating substituents are located para relative to the coordinated nitrogen in the ancillary phen (bpy). These data illustrate clearly that the ancillary ligands are important to the excited-state properties of the complexes. We attribute this observation to the electron-donating substituent pushing the photoexcited electron out onto the phenazine portion of the complex, which results in nonradiative decay.[9,13] This explanation is consistent with previous studies of dppz complexes of Ru(II) in which the incorporation of multiple dppz ligands through the series of complexes $[Ru(phen)_{3-n}(dppz)_n]^{2+}$ caused the Ru(II) emission yield to decrease for $n = 0-3$.[33] The addition of a dppz ligand introduced additional nonradiative decay pathways, presumably by promoting the formation of the phenazine anion. The complex that is outside this trend is $[Os(phen)(dmb)(Me_2\text{-}dppz)]^{2+}$, which has the highest Φ_{em} overall.

(B) Steady-State Emission Yield in the Presence of DNA. Table 6 shows the steady-state emission yield for the family of osmium-based intercalators bound to DNA polymers of various sequences. We also normalized the absolute emission yields against the appropriate Φ_{em} measured in CH_2Cl_2 to account for the inherent emission yield of the complex. By comparing directly the values of this corrected emission yield ($\Phi^{CORR(CH_2Cl_2)}$) for each complex, the effect of the DNA binding environment on the emission yield can be determined. Therefore, the striking differences in emission yield across this series of compounds must result from differences in their interaction with DNA.

For all of the osmium complexes prepared in this study, no luminescence was detected with irradiation of the complex free in aqueous solution. Upon addition of double-helical DNA to a buffered aqueous solution of osmium complex, significant emission was detected over the wavelength range of ~640−840 nm. Occasionally, a preparation of metal complex would display luminescence in buffer free of DNA; however, after rigorously excluding any impurities by HPLC, this background emission was no longer present. The low-energy emission profile, combined with the remarkable sensitivity to the presence of DNA exhibited by the $[Os(phen)_2dppz]^{2+}$ derivatives in aqueous solution makes this class of compounds a unique family of red-emitting DNA probes.

(i) Effects of Structural Modification of the Intercalating Ligand. We first examined the effect of incorporating methyl groups at the 6- (Me-dppz) or the 7,8-positions (Me_2-dppz) of the intercalating dppz ligand. Figure 9A shows the emission spectra as a function of the intercalating ligand for the osmium complexes bound to CT DNA. For this series of complexes, the greatest emission yield is observed for $[Os(phen)_2(Me\text{-}dppz)]^{2+}$, followed by $[Os(phen)_2(Me_2\text{-}dppz)]^{2+}$ and then $[Os(phen)_2(dppz)]^{2+}$.

The sensitivity of the emission yield in these complexes to the environment arises from the fact that proton transfer or hydrogen bond donation from the solvent to the phenazine nitrogens quenches the emission. If one considers the methyl substituent as an electron donor that might drive an excited-state electron off of the phenazine portion of the complex and back into the emissive, tris(phenanthroline) manifold, one would predict that the complex containing Me_2-dppz would have the highest emission yield. However, the Me-dppz ligand produces the brightest emission.[34] Thus, we can attribute a higher emission yield for an osmium intercalator bound to DNA to an increase in protection of these phenazine nitrogens from quenching by solvent that arises from differential interactions with the DNA duplex.

(ii) Effects of Incorporating Substituents on the Ancillary Ligands. Table 6 also lists the Φ_{em} and corrected emission yields for several complexes (in the presence of DNA) that display structural modifications in their ancillary, nonintercalating ligands. We made simple modifications to the ancillary ligands of $[Os(phen)_2(Me_2\text{-}dppz)]^{2+}$ to determine whether these substituents might influence the intercalation of the complexes and affect their emission yield bound to DNA. The Me_2-dppz ligand was chosen as the intercalating ligand owing to its higher emission yield compared with the parent dppz ligand and to the fact that its C_2 symmetry would reduce isomer considerations that could be present with Me-dppz.

The emission spectra for the series $[M(L^1)_2(Me_2\text{-}dppz)]^{2+}$ complexes bound to CT DNA are shown in Figure 9B. Within this series of complexes, we examined (i) the effects of methyl groups at two positions around the perimeter of the phen backbone; (ii) the importance of strongly electron donating substituents such as methoxy and amino groups; and (iii) the role of a carboxylate or methyl ester in the ligand sphere. For $[Os(L^1)_2(Me_2\text{-}dppz)]^{2+}$ complexes in which L^1 = 5,6-dmp or 4,7-dmp, the emission yield is reduced compared with that of the parent L^1 = phen complex. This observation has been made previously for $[Ru(4,7\text{-}dmp)_2(dppz)]^{2+}$,[35] which has a reduced quantum yield for emission in the presence of DNA compared with that of $[Ru(phen)_2(dppz)]^{2+}$.

The difference in the corrected emission yields for L^1 = 5,6-dmp and L^1 = phen in the osmium series is small but significant. When L^1 = 4,7-dmp, the emission yield is reduced dramatically. Such an observation is likely the result of two mechanisms working in tandem. First, the methyl groups at the 4-position prevent the phenazine portion of the dppz ligand from stacking as deeply within the intercalation site as in the phen and 5,6-

(33) Larson, W. Ph.D. Thesis, California Institute of Technology, Pasadena, CA, 1994.

(34) Fees, J.; Kaim, W.; Moscherosch, M.; Matheis, W.; Klima, J.; Krejcik, M.; Zalis, S. *Inorg. Chem.* **1993**, *32*, 166−174.

(35) Stemp, E. D. A.; Arkin, M. R.; Barton, J. K. *J. Am. Chem. Soc.* **1995**, *117*, 2375−2376.

Table 6. Emission Intensities of $[Os(phen)_2(Me_2\text{-}dppz)]^{2+}$ Derivatives Bound to DNA Polymers of Varying Sequence

	DNA Polymer					
	CT (mixed sequence)[b]		poly d(AT)[b]		poly d(GC)[b]	
complex[a]	$\Phi_{em} \times 10^4$ [c]	$\Phi^{CORR(CH_2Cl_2)}$[d]	$\Phi_{em} \times 10^4$ [c]	$\Phi^{CORR(CH_2Cl_2)}$[d]	$\Phi_{em} \times 10^4$ [c]	$\Phi^{CORR(CH_2Cl_2)}$[d]
$[Os(phen)_2(dppz)]^{2+}$	1.00	1.00	0.34	0.34	1.32	1.32
$[Os(phen)_2(Me\text{-}dppz)]^{2+}$	8.75	7.06	5.79	4.76	13.38	10.80
$[Os(phen)_2(Me_2\text{-}dppz)]^{2+}$	6.29	4.26	2.86	1.94	6.54	4.43
$[Os(5,6\text{-}dmp)_2(Me_2\text{-}dppz)]^{2+}$	4.15	3.29	3.25	2.58	2.82	2.23
$[Os(4,7\text{-}dmp)_2(Me_2\text{-}dppz)]^{2+}$	1.03	1.20	0.84	0.98	1.39	1.62
$[Os(dmob)_2(Me_2\text{-}dppz)]^{2+}$	0.15		0.12		0.16	
$[Os(phen)(b'\text{-}OMe)(Me_2\text{-}dppz)]^{2+}$	2.39	1.41	1.34	0.80	2.19	1.29
$[Os(phen)(bpy')(Me_2\text{-}dppz)]^{1+}$	2.55	1.51	1.55	0.92	3.10	1.84

[a] See Table 1 for explanation of ligand abbreviations. [b] Experimental conditions: [Os] = 10 μM, [DNA] = 1 mM nucleotides (Os/nucleotides = 1:100) in buffer (5 mM Tris, 50 mM NaCl, pH = 8.5). Data shown are averages of at least two trials, and uncertainties are estimated to be ±10%. [c] Quantum yield for emission (Φ_{em}) bound to DNA determined by comparison to $[Ru(bpy)_3]^{2+}$ as described previously.[30] [d] Corrected emission yield ($\Phi^{CORR(CH_2Cl_2)} = \Phi_{em}$ bound to DNA divided by Φ_{em} in dichloromethane for each complex. The $\Phi^{CORR(CH_2Cl_2)}$ value allows the emission yields of two complexes to be compared without consideration of the inherent emission yield of the complex. For ease of comparison, these data were normalized to the $\Phi^{CORR(CH_2Cl_2)}$ value for $[Os(phen)_2(dppz)]^{2+}$.

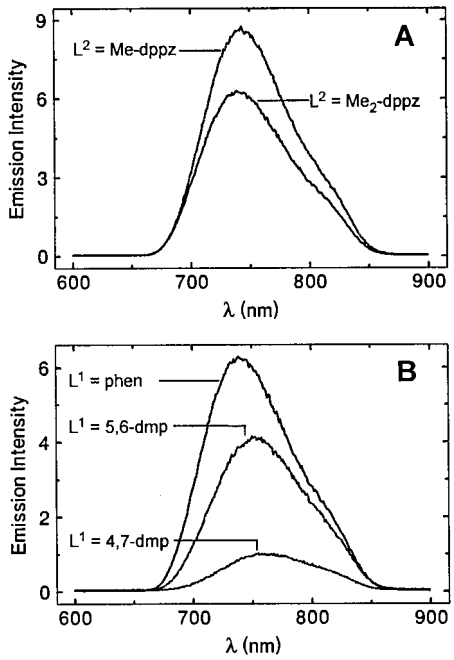

Figure 9. Steady-state emission spectra for $[Os(phen)_2(L^2)]^{2+}$ (A) and $[Os(L^1)_2(Me_2\text{-}dppz)]^{2+}$ (B) complexes bound to CT DNA. Experimental conditions: 10 μM Os, 1 mM nucleotides, 5 mM Tris, 50 mM NaCl, pH 8.5; λ_{exc} = 530 nm. Emission maxima (λ_{max}) are as follows: (A) $L^2 = Me_2\text{-}dppz$, λ_{max} = 731 nm; L^2 = Me-dppz, λ_{max} = 738 nm; (B) L^1 = phen, λ_{max} = 731 nm; L^1 = 5,6-dmp, λ_{max} = 750 nm; L^1 = 4,7-dmp, λ_{max} = 761 nm.

dmp complexes. Second, the 4,7-complex is more sensitive to quenching by water owing to an increase in the excited-state pK_a (the rate of quenching by water in acetonitrile is greater for 4,7-dmp complexes than for 5,6-dmp complexes) at the phenazine nitrogens brought on by the electron-donating substituents on the ancillary ligand. The presence of the methyl groups in the 4,7-positions leads to a stabilization in the Os(III) oxidation state (vide supra), which translates into a more favorable reduction of the phenazine portion of the complex in the excited state. From the structural perspective, substituents at the 4,7-positions may interact disfavorably with the major groove and introduce steric clashes that inhibit effective intercalation. Each of these considerations would increase the sensitivity of photoexcited $[Os(4,7\text{-}dmp)_2(Me_2\text{-}dppz)]^{2+}$ to quenching by water and cause a diminution in emission intensity.

To examine further the importance of electron-donating substituents on the ancillary ligands, we prepared $[Os(dmob)_2(Me_2\text{-}dppz)]^{2+}$ and $[Os(phen)(dab)(Me_2\text{-}dppz)]^{2+}$. We detected no emission for $[Os(phen)(dab)(Me_2\text{-}dppz)]^{2+}$ bound to DNA (Table 6), despite the observation of ~30% hypochromism in the dppz absorption. For $[Os(dmob)_2(Me_2\text{-}dppz)]^{2+}$, the emission yield is significantly reduced. It is well-known that bpy derivatives in the ligand sphere lead to a reduction in emission yield owing to an increase in vibrational deactivation brought about by the flexibility of bpy.[29] For this complex, however, the dramatic loss in emission intensity is almost certainly the result of the electron-donating substituents influencing the sensitivity of the complex to quenching by water. Of course, the methoxy substituents are also in a position to clash sterically with the DNA groove as in the case of 4,7-dmp; however, the loss in intensity for L^1 = dmob is far more dramatic than that with 4,7-dmp. These results illustrate the remarkable sensitivity of luminescent DNA probes based on intercalation of a dppz ligand.

The final issue that we addressed in the investigation of substituents on the ancillary ligands of osmium intercalators was the characterization of the emission of $[Os(phen)(b'\text{-}OMe)(Me_2\text{-}dppz)]^{2+}$ and $[Os(phen)(bpy')(Me_2\text{-}dppz)]^{1+}$. The difference between these complexes lies in the carboxyl substituent on the bpy derivative. For the b′-OMe, the carboxyl is esterified, while a carboxylate is present with bpy′. The carboxylate is deprotonated at pH 8.5 where we conduct our experiments, which results in a net reduction in the overall charge of the metal complex. The key to this study lies in using the difference in charge between the two intercalators to evaluate the relative importance of charge and π-stacking in determining how well these complexes intercalate into DNA.

As shown in Table 6, the emission yield for the bpy′ and the b′-OMe complexes are not significantly different, regardless of DNA sequence. In fact, the emission yield for the bpy′ complex is actually somewhat higher. These data suggest that complexes in this class of intercalators derive their binding affinity for DNA primarily from interactions directly with the DNA base stack through intercalation.

(iii) Sequence Dependence of Emission Yield. We measured the emission intensity of the complexes listed in Table 6 in the presence of three different DNA polymers: calf thymus (CT) DNA; poly d(AT); and poly d(GC). With the exception of $[Os(5,6\text{-}dmp)_2(Me_2\text{-}dppz)]^{2+}$, the sequence dependence of emission intensity for all of the complexes we studied followed the trend Φ_{em} poly d(GC) > Φ_{em} CT > Φ_{em} poly d(AT). In the case of $[Os(5,6\text{-}dmp)_2(Me_2\text{-}dppz)]^{2+}$, we found the emission yield with

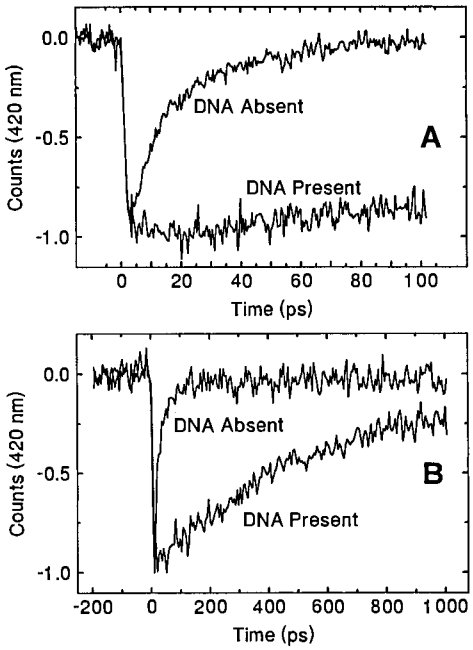

Figure 10. Transient absorption signals on the 100-ps (A) and 1-ns (B) time scales for $[Os(phen)_2(dppz)]^{2+}$ in the presence and absence of CT DNA in aqueous buffer (2 mM nucleotides; 20 μM Os; λ_{exc} = 390 nm, λ_{obs} = 420 nm). In the absence of DNA, the ground-state recovery is biexponential with lifetimes of 9 and 18 ps. In the presence of DNA, the kinetics of ground-state recovery match those of the emission decay (Table 7). Data are normalized. The instrumentation utilized is described in ref 13.

poly d(GC) to be similar to that with poly d(AT), while the emission intensity with CT DNA was the highest.

In previous studies of the interaction of $[Ru(phen)_2(dppz)]^{2+}$ with polynucleotides, we showed that this complex binds preferentially to AT sites in CT DNA.[18] In Table 6, the similarity between the emission intensities for the series of osmium complexes bound to CT and poly d(AT) suggests that the osmium intercalators are preferentially bound to AT sites within CT. This observation illustrates a general feature in the interaction of dppz complexes of transition metals with DNA polymers.

(C) Picosecond Transient Absorption Spectroscopy of $[Os(phen)_2(dppz)]^{2+}$ in the Presence and Absence of DNA. No emission has been detected for $[Os(phen)_2(dppz)]^{2+}$ in aqueous solution. We used transient absorption spectroscopy on the picosecond time scale to characterize the excited-state lifetime of this complex in buffer without DNA. Transient absorption spectroscopy measures the differential absorption for a species before and after a laser pulse. In the case of polypyridyl complexes of Os(II), the excited state is formed within the laser pulse, even for a femtosecond flash.

Owing to the MLCT character of the excited state of $[Os(phen)_2(dppz)]^{2+}$, we expected to see a negative signal that approaches zero over the course of ground-state recovery. Figure 10 illustrates the transient signals observed for $[Os(phen)_2(dppz)]^{2+}$ in the presence and absence of DNA on the 100 ps (A) and 1 ns (B) time scales. As expected, the laser pulse produces a bleach, which recovers to baseline over time. In the absence of DNA, the disappearance of the bleach signal is fast and can be described by two exponential components with lifetimes of 9 and 18 ps. The presence of two components likely reflects the population of more than one MLCT level. In the presence of DNA, however, the lifetime of the complex is significantly enhanced. This observation is consistent with the "molecular light switch" behavior of the steady-state luminescence. Given that, in the presence of DNA (vide infra), the lifetime of the photoexcited complex can be in the range of 10 ns, the presence of DNA produces an enhancement of more than 10^3 in the excited-state lifetime.

(D) Time-Resolved Luminescence of $[Os(phen)_2(dppz)]^{2+}$ Derivatives Bound to DNA. To gain insight into the origins of the variations in emission yield observed for the family of $[Os(phen)_2(dppz)]^{2+}$ derivatives, we measured the excited-state lifetimes for the complexes bound to DNA. We employed both SPC and MPMF to characterize the time-resolved emission decay and found these techniques to give identical results.

Table 7 lists the excited-state lifetimes for the series of osmium intercalators bound to double-helical DNA as a function of nucleic acid sequence. In sharp contrast to the luminescence in CH_2Cl_2, all of the emission decay profiles for the complexes bound to DNA are multiexponential. As described previously for $[Ru(phen)_2(dppz)]^{2+}$,[5,6,16] the multiple components in the luminescence decay of the osmium intercalators bound to DNA are manifestations of more than one geometry of intercalation with respect to the base-pair axis of the binding site.

In general, the average excited-state lifetime is markedly reduced for each complex in the microheterogeneous environment of DNA in aqueous solution. For some complexes, the average excited-state lifetimes track with the lifetimes in CH_2Cl_2. For example, $[Os(4,7\text{-}dmp)_2(Me_2\text{-}dppz)]^{2+}$ has the shortest lifetimes in the presence of DNA, and the profiles of $[Os(5,6\text{-}dmp)_2(Me_2\text{-}dppz)]^{2+}$ $[Os(phen)_2(Me_2\text{-}dppz)]^{2+}$ are very similar in the presence of CT and poly d(AT).

Several noteworthy deviations from the trends established in CH_2Cl_2 are present as well. First, in CH_2Cl_2, the lifetime of photoexcited $[Os(phen)_2(Me_2\text{-}dppz)]^{2+}$ is longest for the series of $[Os(phen)_2(L_2)]^{2+}$ complexes. Bound to DNA, however, the excited-state lifetime of $[Os(phen)_2(Me\text{-}dppz)]^{2+}$ is significantly longer than that of any other complex. Another remarkable contrast is apparent for $[Os(phen)(dmb)(Me_2\text{-}dppz)]^{2+}$ in CH_2Cl_2 and $[Os(phen)(b'\text{-}OMe)(Me_2\text{-}dppz)]^{2+}$ or $[Os(phen)(bpy')(Me_2\text{-}dppz)]^{2+}$, where, bound to DNA, the complexes containing a bpy′ derivative have significantly shorter lifetimes than does the parent dmb complex in CH_2Cl_2. This observation is consistent with the alkyl chain on the bpy′ ligand causing a steric clash with the DNA groove and preventing the phenazine portion of the Me_2-dppz ligand from intercalating as deeply into the base stack.

Time-resolved emission spectroscopy is useful to identify subtle differences in the way luminescent compounds associate with DNA. An example of this application lies in the comparison of the emission of $[Os(phen)(b'\text{-}OMe)(Me_2\text{-}dppz)]^{2+}$ and $[Os(phen)(bpy')(Me2\text{-}dppz)]^{2+}$ bound to CT DNA. For these two complexes, the steady-state emission yields are almost identical; however, the time-resolved profiles reveal important differences. Bound to CT DNA, the lifetimes of the bpy′-containing complex are significantly shorter than those of the b′-OMe. Such an observation is likely derived from the negative charge on the bpy′, which prevents the complex from intercalating as deeply as does the complex with the methyl ester. The fact that the steady-state yields are similar results from a change in the distribution of lifetimes in the multiexponential decay in favor of the long lifetime.

(i) Effect of DNA Sequence on Luminescence Lifetime. As indicated in Table 7, the luminescence lifetimes for the osmium intercalators bound to DNA depend significantly on the sequence of the polymer. In general, the distribution and magnitude of the lifetimes for the complexes bound to CT DNA

Table 7. Luminescence Lifetimes (τ in ns) of Dipyridophenazine Complexes of Os(II) Bound to Natural and Synthetic DNA Polymers

	DNA Polymer							
	CT (mixed sequence)[b]			poly d(AT)[b]			poly d(GC)[b]	
complex[a]	τ1 (%)[c]	τ2 (%)[c]	τ3 (%)[c]	τ1 (%)[c]	τ2 (%)[c]	τ3 (%)[c]	τ1 (%)	τ2 (%)
$[Os(phen)_2(dppz)]^{2+}$	14.9 (10.0)	2.9 (28.9)	0.8 (61.2)				5.0 (54.1)	1.1 (45.9)
$[Os(phen)_2(Me\text{-}dppz)]^{2+}$	49.8 (12.9)	19.9 (46.6)	4.1 (40.5)	28.7 (34.7)	9.9 (29.0)	3.8 (36.3)	28.5 (48.9)	8.1 (51.1)
$[Os(phen)_2(Me_2\text{-}dppz)]^{2+}$	34.8 (10.4)	11.1 (32.3)	2.9 (57.3)	23.6 (10.0)	4.6 (57.4)	0.8 (32.7)	19.7 (26.6)	4.0 (73.4)
$[Os(4,7\text{-}dmp)_2(Me_2\text{-}dppz)]^{2+}$	6.4 (31.4)	2.0 (68.6)		3.9 (59.3)	1.6 (40.7)		9.2 (36.7)	1.4 (63.3)
$[Os(5,6\text{-}dmp)_2(Me_2\text{-}dppz)]^{2+}$	30.1 (7.3)	10.0 (36.9)	2.3 (55.7)	25.2 (7.3)	10.7 (31.4)	2.9 (61.3)	11.3 (29.7)	2.2 (70.3)
$[Os(phen)(b'\text{-}OMe)(Me_2\text{-}dppz)]^{2+}$	23.4 (6.5)	6.9 (37.0)	1.7 (56.5)	8.3 (23.9)	2.2 (76.1)		11.5 (30.3)	2.2 (69.7)
$[Os(phen)(bpy')(Me_2\text{-}dppz)]^{2+}$	15.1 (13.7)	4.3 (51.2)	1.4 (35.1)	6.2 (39.3)	2.1 (60.7)		11.1 (31.0)	2.3 (69.0)

[a] See Table 1 for explanation of ligand abbreviations. [b] Experimental conditions: [Os] = 30 μM; [DNA] = 3 mM nucleotides (Os/nucleotides = 1:100) in buffer (5 mM Tris, 50 mM NaCl, pH = 8.5). For data collected by single photon counting, (SPC) λ_{exc} = 670 nm, λ_{obs} = 740 nm. Data fitting achieved by nonlinear least-squares method using commercial software (ISS (MPMF); AXUM (SPC)). Error in lifetime and % contribution is estimated at ±10%. [c] % contribution corresponds to the ratio of the appropriate preexponential factor to the sum of such factors, normalized to 100%.

resemble very closely those in the presence of poly d(AT). The longest lifetimes are observed with CT DNA. Bound to poly d(GC), the excited-state decays can all be described as biexponential, with the majority of the luminescence coming from the population with the shortest lifetime. When the complexes are bound to poly d(GC), the individual excited-state lifetimes are shorter compared with data for the other two sequences, despite greater steady-state emission yields bound to poly d(GC). This apparent disparity arises because the average excited-state lifetime with poly d(GC) is greater, so even though the individual lifetimes are shorter, the emission yield is higher.

Previous studies of $[Ru(phen)_2(dppz)]^{2+}$ luminescence as a function of DNA sequence revealed that this complex binds preferentially to AT sites.[18] For the family of complexes in this study, the luminescence data with CT are more similar to the data with AT rather than GC. However, in the presence of CT, the longest lifetime is usually significantly longer than with AT; therefore, the complexes are likely binding at sites that are not simply either AT or GC but at sites that reflect the heterogeneity of the sequence of CT DNA.

(ii) Luminescence Lifetimes of Δ- and Λ-$[Os(phen)_2(dppz)]^{2+}$ Bound to CT DNA. We measured the luminescence lifetimes of the pure enantiomers of $[Os(phen)_2(dppz)]^{2+}$ bound to DNA in order to investigate the role of absolute configuration about the metal center in determining the luminescence lifetimes of the complexes bound to DNA. Owing to the right-handed chirality of the DNA duplex, we expected the interaction of the right-handed Δ-isomer to be favored.[36] Indeed, a large body of evidence illustrates that the interaction of metallointercalators with DNA is favored for the Δ-isomer on the basis of symmetry matching and shape selection.[1,2,36]

For both enantiomers of this complex, the luminescence decay can be described by a biexponential function. For Δ-$[Os(phen)_2(dppz)]^{2+}$, the decay contains 24% of a 9.2 ns component and 76% of a 1.5 ns component. For the Λ isomer, the lifetimes are significantly shorter. The decay profile for this complex consists of a 70% contribution by a 750 ps component and a 30% contribution by a 1 ns component. These data for the pure enantiomers were recorded at a ratio of 1:100, Os/nuc. The excited-state lifetimes, and hence the quantum yield for emission, are much greater for the Δ isomer of this complex compared with those for the Λ isomer. Importantly, when taken as a linear combination, the time-resolved emission profiles for the pure enantiomers of $[Os(phen)_2(dppz)]^{2+}$ are consistent with the data recorded for the racemic mixture.

(E) Low-Temperature Luminescence Studies. To determine whether $[M(phen)_2(dppz)]^{2+}$ complexes might be useful in studying reactions with DNA at low temperature, we measured the luminescence lifetimes of $[Os(phen)_2(dppz)]^{2+}$ in the presence and absence of DNA at 77 K (Figure 11). The solvent used was a mixture of glycerol and buffer.

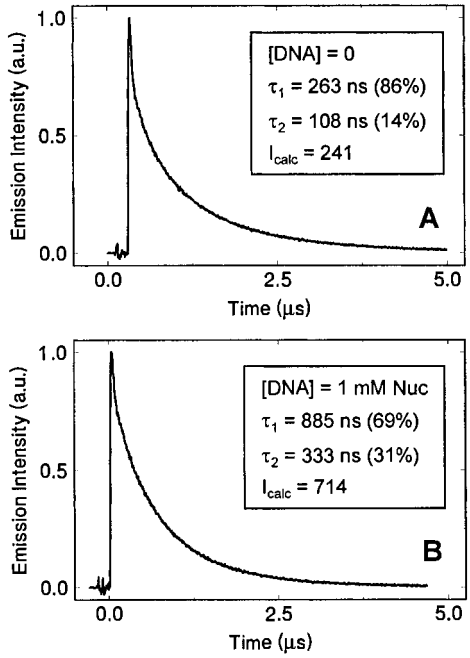

Figure 11. Time-resolved luminescence decay of $[Os(phen)_2(Me_2\text{-}dppz)]^{2+}$ in the absence (A) and presence (B) of DNA at 77 K. Experimental conditions: 15 μM Os, 1.5 mM nucleotides, 5 mM Tris, 50 mM NaCl, pH 8.5 in 60% glycerol, 40% water; λ_{exc} = 480 nm, λ_{obs} = 740 nm. Samples were contained in NMR tubes and frozen slowly in liquid N_2, which did not always provide for uniform glasses; instead the solid was a heterogeneous mixture of frozen sections.

At ambient temperature, the osmium emission is quenched in the cryosolvent. At 77 K, however, the complex emits strongly, even in the absence of DNA (Figure 11). This observation suggests that quenching of the excited state by the interactions of protons with the phenazine nitrogens is inhibited at low temperature. It is noteworthy that in the absence of DNA, the excited state decays as a biexponential. This observation resembles the data at ambient temperature in aqueous solution.

In the presence of DNA at 77 K, the emission of the osmium decays also as a biexponential; however, the lifetimes are enhanced relative to those in the absence of DNA. The observation of enhanced lifetime in the presence of DNA suggests that the complex remains bound to DNA even at 77 K in the cryosolvent.

(36) Barton, J. K. *Science* **1986**, *233*, 727−734.

Discussion

Synthetic Methods. The preparation of mixed-ligand complexes of Os(II) and Ru(II) has been the subject of considerable interest for many years, dating back to the work of Dwyer and co-workers.[25−27,37] We employed these strategies to prepare complexes of the $[Os(L^1)_2(L^2)]^{2+}$ type. Until recently, no methods for the preparation of polypyridyl complexes of osmium bearing three different bidentate ligands had been described. We developed the simple strategy outlined in Scheme 2 as a general approach to obtain complexes of the $[Os(L^1)(L^2)(L^3)]^{2+}$ type. With this method, we are able to introduce one bidentate polypyridyl ligand onto the osmium center, selectively without overreaction.

We found that the key to this approach is the incorporation of the second ligand onto $[Os(phen)Cl_4]$ in DMF. In solvents such as ethylene glycol, heating the mixture results in the incorporation of two ligands onto the metal center. We suspect that the selectivity in this reaction arises from the role that the solvent plays in reducing the osmium center, which affects the lability of the chloride ligands. The lower oxidation state of the metal center is more susceptible to loss of chloride, and therefore more reactive. Both DMF and ethylene glycol (at reflux) will reduce Os(IV) to Os(III) and Os(III) to Os(II); however, DMF must be less reactive than ethylene glycol in this regard and prevents the accumulation of Os(II) while there is an excess of bidentate ligand in solution. This methodology is convenient and general. We have employed it to prepare a variety of complexes with many functionalities present on the coordinating phen, bpy, or dppz derivatives.

Electronic Structure of Ground-State $[Os(phen)_2(dppz)]^{2+}$ Derivatives. The assembly of several dppz complexes of Os(II) and the characterization of their electrochemical properties have allowed us to develop a picture of the electronic structure of these complexes. We find that substituents on the phen or bpy ligands of the complex affect the reduction potential of the metal center but not the phenazine portion of the dppz ligand. By contrast, substituents on the 6- or 7,8-positions of the dppz ligand perturb the reduction potential of the phenazine portion of the ligand but not the metal center. This orbital arrangement may be unique because one has independent, modular control in tuning the energetics of two different states simultaneously.

Excited-State Properties in the Absence of DNA. Role of Ligand Architecture in Determining Φ_{em} in Dichloromethane. The presence of the dppz ligand in complexes of Ru(II) and Os(II) introduces a significant perturbation in the excited-state properties of complexes with this ligand.[9,12,13] Increasing the number of dppz ligands in $[Ru(phen)_n(dppz)_{3-n}]^{2+}$ complexes resulted in a decrease in Φ_{em} in acetonitrile.[33] For complexes of Re(I), the similarity in the absolute energy of the MLCT transition and the $\pi-\pi^*$ transition centered on the dppz ligand results in quenching of the MLCT state by intersystem crossing to the $\pi-\pi^*$ state.[7,8,38]

The dependence of the emission yield on ligand architecture for the $[Os(phen)_2(dppz)]^{2+}$ derivatives in CH_2Cl_2 is clearly illustrated in Table 5. The presence of electron-donating substituents on the ancillary phen or bpy ligand results in a decrease in the emission yield, while the presence of electron-donating substituents on the dppz derivative causes Φ_{em} to increase. This trend is consistent with a model that involves IMCT to a deactivating state. When a substituent drives electron density into the metal center, crossover to the phenazine portion of the dppz ligand, which results in nonradiative deactivation of the excited state, is favored. Alternatively, when the reduction potential of the phenazine portion of the molecule is disfavored by an electron-donating substituent, this pathway of nonradiative decay is inhibited.

Therefore, the bis-phen and bis-5,6-dmp complexes display similar Φ_{em} values, while the bis-4,7-dmp complex has a shorter excited-state lifetime in CH_2Cl_2. The most electron donating ligand is the dmob ligand, and complexes with this ligand have the lowest emission yield overall.

For the series of dppz derivatives with two phen ligands, the lowest Φ_{em} in CH_2Cl_2 is observed for dppz, followed by Me-dppz, and, in CH_2Cl_2, complexes with the Me_2-dppz ligand have the highest Φ_{em}. This trend is consistent with the hypothesis that the transfer of electron density from the excited state to the dppz ligand quenches emission, since the electron-donating methyl groups reduce the electron-accepting character of the phenazine moiety.

Last, if one considers the excited state as an MLCT state with substantial electron density localized on the dppz ligand as described previously by Meyer and co-workers,[31] the differences in Φ_{em} observed for the series of complexes in CH_2Cl_2 also follow the trend predicted by the energy gap law.[31] It is also clear that the ancillary ligands contribute to the excited-state structure, again consistent with perturbations in the excited-state energy gap leading to the ligand-dependent Φ_{em}. Therefore, in nonaqueous solution, the family of dppz complexes of Os(II) display excited-state lifetimes that show a strong dependence on the structure of all three coordinating ligands.

Correlations between Absorption and Emission Data and the Effect of Substituents on DNA Binding. Structural Modification of the Intercalating Ligand. We considered first the importance of substituents on the intercalating, dppz derivative. Owing to its flat, expansive aromatic surface, the dppz ligand is well-suited for intercalation between adjacent DNA base pairs. Studies of DNA binding by UV−vis spectroscopy indicate that the association of dppz complexes of Os(II) proceeds by preferential intercalation of the dppz derivative, which protects the phenazine nitrogens from solvent. Therefore, the complexes emit in the presence of DNA.

According to the inherent excited-state properties in CH_2Cl_2 (Table 5), one would expect $[Os(phen)_2(Me_2\text{-}dppz)]^{2+}$ to have the brightest emission bound to DNA, however, the complex with Me-dppz has the greatest Φ_{em} overall. This observation indicates that the Me-dppz complex is intercalated with the phenazine nitrogens deeper in the DNA base stack, and more protected from quenching by water. If we look at the time-resolved luminescence data (Table 7), we see that not only are the individual lifetimes in the triexponential decay longer but the distribution of the lifetimes shifts from favoring the shorter lifetime in the dppz complex to favoring a significantly longer intermediate ($\tau 2$) lifetime in the Me-dppz complex.

One consideration could be that the excited-state pK_a of the phenazine nitrogens is responsible for the differences in emission yield. Owing to the electron-donating nature of the methyl groups on the phenazine portion of the dppz ligand, the phenazine nitrogens should increase in basicity going from dppz to Me-dppz to Me_2-dppz. If this hypothesis were correct, dppz would give the brightest emission followed by Me-dppz and Me_2-dppz, which is inconsistent with the data.

Effect of Functional Groups on the Ancillary Ligands. We suggest that the primary trend with respect to the role of ligand architecture in determining DNA binding lies in the regiochem-

(37) Anderson, P. A.; Deacon, G. B.; Haarmann, K. H.; Keene, F. R.; Meyer, T. J.; Reitsma, D. A. *Inorg. Chem.* **1995**, *34*, 6145−6157.
(38) Worl, L. A.; Rich, D.; Chen, P.; Ciana, L. D.; Meyer, T. J. *J. Chem. Soc., Dalton Trans.* **1991**, 849−858.

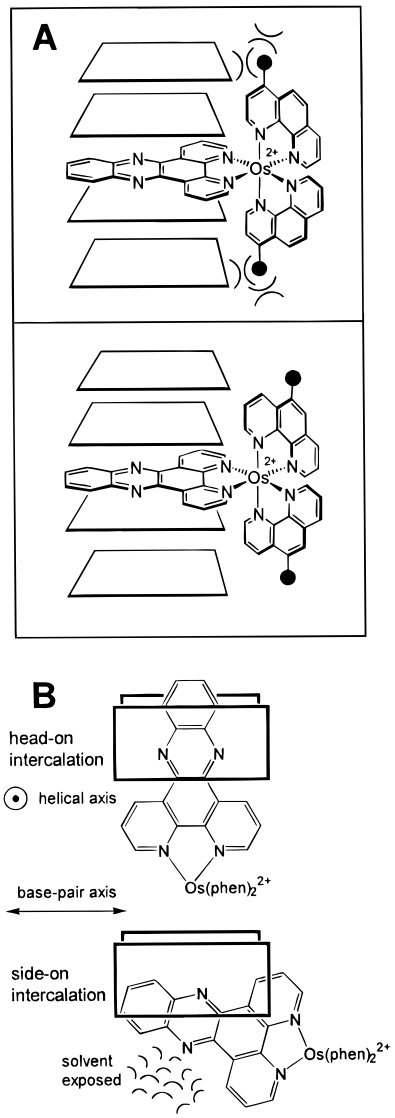

Figure 12. (A) Schematic illustration of two metallointercalators bound to DNA. In the upper panel, the substituents on the 4-positions of the ancillary phen ligands clash with the wall of the groove and prevent deep penetration of the dppz ligand into the DNA base stack. In the lower panel, the substituents on the 5-positions are much more innocuous and allow the dppz ligand to intercalate further into the hydrophobic base stack. (B) Schematic illustration of $[Os(phen)_2(dppz)]^{2+}$ bound to a base pair in the head-on (top) and side-on (bottom) modes of intercalation. Intercalation by the head-on mode results in the phenazine nitrogens being deeper in the base stack and shielded from solvent. The side-on mode causes the phenazine nitrogens to be more solvent exposed.

istry of substitution. Our data show quite convincingly that substituents on the 4- and 7-positions of a phen ligand (4- and 4′-positions on bpy) cause a reduction in emission yield, and a diminution of the hypochromicity associated with intercalation. As depicted schematically in Figure 12, substituents on the 4-position of an ancillary phen ligand can cause steric clashes with the wall of the major groove into which the complexes are intercalating. Such steric clashes would not be present with substituents on the 5- and 6-positions. Therefore the diminished hypochromicity results from intercalation where the phenazine chromophore does not overlap as much with the DNA base pairs, which may also affect the K_B. The lower emission yield results from less protection of the phenazine nitrogens from solvent incurred by the relative decrease in overlap of the dppz ligand with the base stack.

Reconciling Emission Data with Models of Intercalation. Previous models of intercalation by dppz complexes assert that each lifetime in the multiexponential decay corresponds to a geometry of intercalation which provides differential exposure of the phenazine nitrogens to water (Figure 12).[5,6,16−18] The two extremes for the different orientations in this model are head-on and side-on intercalation. For the head-on mode, the phenazine nitrogens are placed deeper in the helix and thus shielded from the solvent. For side-on, the dppz ligand is more exposed to water. In the context of this model, the differences in the luminescence decays for the series of complexes bearing different substituents on the intercalating ligand would indicate that the presence of methyl groups on the 6- or 7,8-positions of dppz forces the complexes to adopt different geometries of intercalation. One could imagine that the fact that the Me-dppz complex displays the greatest Φ_{em} indicates that the methyl substituent at the 6-position forces the complex to adopt an intercalation geometry which buries the phenazine nitrogens in the hydrophobic interior of the base stack.

Given that intercalative binding is driven by the stacking interaction with the bases, the predominant mode of binding in a head-on vs side-on competition would be side-on. As illustrated in Figure 12, a side-on orientation provides a greater surface area for intercalative stacking; protection of the phenazine nitrogens from solvent does not provide any binding energy. In fact, the time-resolved emission data do support the idea of side-on intercalation being preferred. The shorter relative lifetimes dominate the decay profiles of all the complexes, including the pure enantiomers.

Another model proposed to account for the multiexponential decay invokes a distribution effect,[32] where the presence of more than one excited-state lifetime for the intercalated complex arises from the fact that some complexes may bind in the vicinity of others and shield the complexes from solvent. In this study we have concentrated on only one binding density. Nonetheless, our data appear to be inconsistent with such a model. For example, the $[Os(phen)_2(Me_n\text{-dppz})]^{2+}$ ($n = 0-2$) complexes, where only the intercalating ligand changes, display wide variations in their time-resolved luminescence decays. We suggest that the multiexponential decays observed for the intercalators based on Os(II) and Ru(II) instead reflect population of more than one intercalated geometry. These differing geometries would result in differential exposure of the phenazine nitrogens to solvent. While photophysical data solely cannot be used to arrive at a firm conclusion concerning the structure of these complexes bound to DNA, it is noteworthy that NMR studies are also consistent with such a model.[14,15]

Sequence-Dependent Solvent Accessibility of Intercalated Os(II) Complexes. Since the emission profile of a dppz complex of Os(II) depends so sensitively upon solvent accessibility, we can ask how solvent accessibility varies as a function of DNA sequence. Establishing trends in how sequence predisposes a compound to be solvent-exposed upon intercalation may lend insight into the reactivity of molecules with DNA. The solvent accessibility of an agent bound to DNA is an important property of the DNA−drug complex. Species that are tightly bound to DNA and show very little accessibility to solvent are less prone to reactions with exogenous species in solution. Conversely, when the DNA−drug complex is open to solvent, the reactivity of the binding agent with diffusible reactants in solution may be exploited to initiate chemistry on the DNA helix.

The best measure of solvent accessibility for dppz complexes of Os(II) is the excited-state lifetime of the metal complex bound to DNA. If we focus on a complex like $[Os(phen)_2(Me_2\text{-}$

dppz)]$^{2+}$, we find that the longest lifetimes are observed with CT DNA followed by poly d(AT), while the longest lifetime in the presence of poly d(GC) is significantly reduced compared with the other polymers. So even with a binding mode that favors shielding from solvent, this shielding is sequence-dependent.

If we focus on the lifetimes of photoexcited [Os(phen)$_2$(Me$_2$-dppz)]$^{2+}$ that contribute the most to the overall decay profile, we see that the lifetimes are shortened for the complex bound to poly d(AT), followed by CT DNA, and then poly d(GC). In fact, for the GC polymer, the decay is biexponential, while with CT and poly d(AT), the excited states decay as triexponentials. This distinction suggests that the sequence affects the orientation of intercalation so significantly that the mode of binding that gives the maximum exposure to solvent is not present for poly d(GC). Therefore, despite the fact that poly d(AT) and CT DNA provide orientations for intercalation that maximize protection from solvent, the average complex bound to poly d(GC) is the most protected from water.

Summary and Conclusion

By incorporating simple modifications in the ligand sphere of several dppz complexes of Os(II), the fundamental excited-state properties of these complexes in nonaqueous solvents were characterized. The presence of electron-donating substituents that lower the third ionization potential of the osmium metal center leads to a reduction in the Φ_{em} in CH_2Cl_2 by forcing electron density onto the phenazine portion of the dppz derivative. Conversely, electron-donating substituents on the 6 or 7,8-positions of the dppz derivative raise Φ_{em} by pushing electron density off this ligand. In the presence of DNA, the emission properties of the complexes depend very significantly on their ligand architecture. The differences in emission yields and lifetimes for the complexes bound to DNA reflect differences in binding orientation and solvent accessibility in the metallointercalator−DNA complex. The emission properties, and hence binding properties, depend on the DNA sequence as well. Overall, dppz complexes of Os(II) provide a class of red-emitting intercalators that are sensitive to the ligand sphere around the metal as well as to the composition of the matrix to which they are associated. Such a family of metallointercalators provides a foundation to develop sensitive diagnostics for nucleic acids in solution.

Acknowledgment. We are grateful to the NIH (GM33309) for financial support of this work, the Ralph M. Parsons Foundation for a predoctoral fellowship (R.E.H.), and Caltech for a summer undergraduate research fellowship (J.A.Y.). We also thank Prof. P. F. Barbara and E. J. C. Olson for their assistance in obtaining picosecond transient absorption data.

Supporting Information Available: ^{1}H NMR spectrum of [Os(phen)(Me$_2$-dppz)Cl$_2$] in CD_2Cl_2; ^{1}H NMR spectrum of [Os(phen)(bpy′)(Me$_2$-dppz)]$^{2+}$ in CD_3OH; CD spectra of the pure enantiomers of [Os(phen)$_2$(dppz)]$^{2+}$ in water (4 pages). Ordering information is given on any current masthead page.

IC9808955